atoms

MDPI

Article

Spin Asymmetry for the Elastic Scattering of Polarized Electrons from Zn, Cd, and Hg

Mehrdad Adibzadeh [1,*] and Constantine E. Theodosiou [2]

[1] Department of Physics, University of West Florida, Pensacola, FL 32514, USA
[2] Department of Mathematics and Physics, Manhattan University, Riverdale, NY 10471, USA; constant.theodosiou@manhattan.edu
* Correspondence: madibzadeh@uwf.edu

Abstract

We present an extensive set of theoretical results for spin asymmetry in the form of Sherman functions for the elastic scattering of electrons by zinc, cadmium, and mercury. This study extends the application to these three atoms of our earlier method of calculations, previously employed for stable inert gases and alkaline-earth metals. Our predictions are in adequate agreement with experimental values and precise theoretical results and extend the available theoretical data to a large impact energy range.

Keywords: elastic electron scattering; spin asymmetry; zinc; cadmium; mercury

PACS: 34.80.Bm

1. Introduction

The investigation of electron spin asymmetry in elastic electron scattering from atoms illustrates the extent of spin-dependent interactions in electron–atom collisions. In the case of closed-shell atoms, which represent spin-zero targets, the spin asymmetry effects are due to the spin–orbit interactions. Thus the theoretical studies of spin asymmetry in elastic scattering from heavy closed-shell atoms, such as zinc, cadmium and mercury, with zero total angular momentum, signify the subtleties of relativistic effects and the antisymmetrization of the wave function.

Among the three atoms, mercury is the most studied through atomic collisions, particularly due to its industrial applications. Zinc and cadmium have been experimentally studied to a lesser extent. The early studies of electron–atom scattering were concentrated on obtaining cross sections. The studies into spin polarization effects followed later on with renewed interest in both experimental and theoretical approaches.

For zinc, there is only one experimental work on the study of spin polarization of elastically scattered electrons, that of Bartsch et al. [1] for energies up to 14 eV. The theoretical investigations on this subject are those of McEachran and Stauffer [2], Kumar et al. [3], Szmytkowski and Sienkiewicz [4], and Bostock et al [5].

In the case of cadmium, the only experimental work is that of Bartsch et al. [1] for energies up to 9 eV. The body of theoretical elastic spin asymmetry calculations on cadmium includes the works of Nahar [6], McEachran and Stauffer [2], Kumar et al. [3], Szmytkowski and Sienkiewicz [4], Berrington et al. [7], and Haque et al [8].

Mercury, in contrast, has enjoyed more attention from experiments and theory. There exist several spin polarization experimental investigations of elastically scattered electrons.

Check for updates

Academic Editors: Harindranath Ambalampitiya and Robyn Wilde

Received: 28 April 2026
Revised: 1 July 2026
Accepted: 9 July 2026
Published: 14 July 2026

Copyright: © 2026 by the authors. Licensee MDPI, Basel, Switzerland. This article is an open access article distributed under the terms and conditions of the Creative Commons Attribution (CC BY) license.

They include the works of Deichsel [9], Jost and Kessler [10], Deichsel et al. [11], Eitel et al. [12], Eitel and Kessler [13], Hanne et al. [14], Düweke et al. [15], Albert et al. [16], Hanne et al. [17], Berger et al. [18], Möllenkamp et al. [19], Berger and Kessler [20], Kaussen et al. [21], and Dümmler et al [22]. The theoretical calculations of the subject include those of Bunyan [23], Bunyan and Schonfelder [24], Fink and Yates [25], Bartschat et al. [26], Haberland and Fritsche [27], McEachran and Stauffer [28], Sienkiewicz [29], Fritsche et al. [30], Szmytkowski and Sienkiewicz [4], Kelemen and Remeta [31], and Haque et al. [8,32].

The present authors have studied these processes theoretically for inert gases and quasi-two-electron stable alkaline-earth metal atoms [33–35] with considerable success. The method is a fully relativistic approach that uses a Dirac–Slater central potential to represent the target atom, supplemented by an exchange and a target polarization potential. Our (single-channel) approach enables studies at high energies, not easily treated by multi-channel approaches. This work is an application of our approach to Group 12 atoms, i.e., Zn, Cd, and Hg, which are also quasi-two-electron atoms.

2. Brief Review of the Theoretical and Computational Approach

When a partially polarized beam of electrons is elastically scattered from atoms, the study of the angular distribution of the scattered electrons displays important information about the beam–target interaction. In the general case, a partially polarized electron beam is characterized by its *polarization* P, defined [36] as

$$P = \frac{n_{\text{up}} - n_{\text{down}}}{n_{\text{up}} + n_{\text{down}}}, \tag{1}$$

where n_{up} and n_{down} are the number of electrons with spin up and spin down, respectively, with respect to a chosen axis. The scattered electrons are characterized by their *asymmetry* A, given by

$$A = \frac{n_R - n_L}{n_R + n_L}, \tag{2}$$

where n_R and n_L are the number of electrons deflected to the right and to the left of the incident beam, respectively. A simple expression between A and P was derived by Sherman [37]

$$A = PS(\theta)\,, \tag{3}$$

where $S(\theta)$ is a measure of the probability a spin-up electron will be scattered at an angle θ with respect to the polarization axis due to spin–orbit interactions [38,39]; its values range from -1 to +1. The Sherman function (SF) $S(\theta)$ is also expressed in terms of scattering amplitudes as [37,38]

$$S(\theta,k) = i\frac{f(\theta,k)g^*(\theta,k) - f^*(\theta,k)g(\theta,k)}{|f(\theta,k)|^2 + |g(\theta,k)|^2}, \tag{4}$$

where f and g are the direct and spin–flip scattering amplitudes, respectively:

$$f(\theta,k) = \frac{1}{k}\sum_{l=0}^{\infty}\left[(l+1)e^{i\delta_l^+(k)}\sin\delta_l^+(k) + le^{i\delta_l^-(k)}\sin\delta_l^-(k)\right]P_l(\cos\theta)\,, \tag{5}$$

and

$$g(\theta,k) = \frac{1}{k}\sum_{l=0}^{\infty}\left[e^{i\delta_l^-(k)}\sin\delta_l^-(k) - e^{i\delta_l^+(k)}\sin\delta_l^+(k)\right]P_l^1(\cos\theta)\,. \tag{6}$$

In the above equations, k and θ are the wave number of the incident electron and the scattering angle, respectively.

https://doi.org/10.3390/atoms14070057

In this work, we apply the same method of calculations as that described in our previous papers [33–35], i.e., the standard method of partial-wave expansion in potential scattering. We obtained the necessary phase shifts by solving the stationary Dirac equation, for which the choices of central static atomic, exchange, and polarization potentials were determined through an extensive analysis. The present choices for the particular form of those potentials were determined to be the same as those of Refs. [34,35]. To determine the combination for potentials, we performed an exhaustive analysis and comparison with the collection of all appropriate experimental and theoretical results on elastic electron scattering by inert gases and alkaline-earth metals. As a result we were able to recommend a combination of the central static atomic, exchange, and polarization potentials, which produced a consistent agreement between our calculated cross sections and reliable experimental and theoretical results at different projectile energies.

Our analyses showed that the most consistent combination of potentials for Zn, Cd, and Hg was to be the Dirac–Slater atomic potential $V_S(r)$ [40], the semi-classical exchange potential expression by Furness and McCarthy [41]

$$V_E(r) = \frac{1}{2}\Big[|E - V_S(r)| - [|E - V_S(r)|^2 + 4\pi\rho(r)]^{\frac{1}{2}}\Big], \tag{7}$$

and the polarization potential [42,43] in the form

$$V_P(r) = -\frac{\alpha_d}{2(r^2 + r_c^2)^2}\,. \tag{8}$$

In the above equation, α_d and r_c are the static atomic polarizability and the cutoff radius, respectively. The static polarizabilities were taken from the theoretical values of Kolb et al [44]. They are 50.8 a_0^3, 63.7 a_0^3 and 44.9 a_0^3 for Zn, Cd, and Hg respectively.

In the present work, we applied the same diligence to confirm for Zn, Cd and Hg our earlier choices for the cutoff radius of the polarization potential, the only free parameter in our calculations. Similar to our previous works, we required r_c to be a smooth, continuous and finite function of the scattered electron energy E. We further confirmed the functional behavior of this energy-dependent cutoff radius to be similar to those we used for alkaline-earth-metal atoms [34,35] through comparisons with dependable theoretical and experimental data. Our careful analysis determined the value for the cutoff radius for zinc to be (in atomic units)

$$r_c(E) = \begin{cases} \frac{1}{3}\ln(\frac{E}{\mathcal{R}}) + \langle r\rangle_{4s} & E \geq 45 \text{ eV}, \\ \\ 3.85 & E < 45 \text{ eV}, \end{cases} \tag{9}$$

for cadmium,

$$r_c(E) = \begin{cases} \frac{1}{3}\ln(\frac{E}{\mathcal{R}}) + \langle r\rangle_{5s} & E \geq 30 \text{ eV}, \\ \\ 4.0 & E < 30 \text{ eV}, \end{cases} \tag{10}$$

and for mercury,

$$r_c(E) = \begin{cases} \frac{1}{3}\ln(\frac{E}{\mathcal{R}}) + \langle r\rangle_{6s} & E \geq 20 \text{ eV}, \\ \\ 3.6 & E < 20 \text{ eV}. \end{cases} \tag{11}$$

Here E is the energy of the incident electron in eV, $\mathcal{R}$ is the Rydberg constant ($\mathcal{R}$ = 13.605 691 72 eV), and $\langle r\rangle_{4s} = 2.680\, a_0$, $\langle r\rangle_{5s} = 2.978\, a_0$ and $\langle r\rangle_{6s} = 3.045\, a_0$ are the expectation values of zinc's 4*s* shell, cadmium's 5*s* shell, and mercury's 6*s* shell radii, respectively. The cutoff radii for low energies are set to constant values to avoid the

anomaly caused by the logarithmic term. For more discussion on this constant value and its behavior below an energy threshold, the reader may consult Ref. [34]. Additionally, to obtain the low-energy constant values for r_c, comparisons with accurate theoretical data for an integrated cross section were also used as guidance. Similar to our previous works, we used our modified version of the code by Salvat et al. [40] in our calculations. Our modifications to the code include the addition and testing of the efficacy of several forms of exchange and polarization potentials. It is worth mentioning that the radial numerical integration for all three atoms extended to about 1000 a_0, depending on the static atomic potential's drop-off radius. Throughout this work and for all considered energies, we used up to 150 partial-wave phase shifts.

Once the Dirac Hamiltonian is determined and the Dirac equation is solved, we obtain the needed spin-up δ_l^+ and spin-down δ_l^- phase shifts, which are in turn used to determine the direct, f, and spin–flip, g, scattering amplitudes.

3. Results and Discussion

We would like to compare our results with all available experimental measurements and theoretical works. Yet, to maintain graph readability, we will limit the comparisons to the most recent and reliable data whenever possible. Furthermore, we avoid the placement of error bars on experimental data if the uncertainty may be engridled by means of an appropriate size of the marker. Lastly, the calculated Sherman functions produced in this work are available through Supplementary Materials in electronic format.

3.1. Zinc

The experimental data on spin asymmetry for elastic electron scattering off zinc are limited to those of Bartcsh et al. [1] for a few energies between 2 eV and 14 eV. At impact energies for which experimental data are available, we compare our Sherman functions with the experiment and other theoretical results in Figures 1 and 2. These comparisons include the relativistic distorted-wave (RDW) calculations of McEachran and Stauffer [2] and Szmytkowski and Sienkiewicz [4] and the 66-state relativistic convergent close coupling (RCCC) formulation of Bostock et al. [5].

The present Sherman function values at 2 eV impact energy are in outstanding agreement with the experiment, as seen in Figure 1. This agreement is to a lesser extent on display at 3 eV as well. Nonetheless, the agreement of our Sherman functions at 4 and 5 eV with the experiment is mostly limited to the forward direction, while the RCCC calculations present excellent agreement with the experiment. For impact energies of 6 and 9 eV, in Figure 2, our Sherman functions again show excellent agreement with the experiment and the RCCC results in the forward direction. Both RDW calculations at 9 eV indicate a considerable disagreement with the experiment.

The most interesting comparisons, however, are those at 11 and 14 eV impact energies in Figure 2. At 11 eV, our values show a much better agreement with the experiment than those of the RCCC calculations. As touched upon by Ref. [5], the discrepancy between the RCCC Sherman function and the experiment at 11 eV is due to $3d^{10}$ excitations, which were not modeled accurately by the RCCC formalism. Considering our single-channel method of calculations does not include the effects of excited states on elastic spin asymmetry, our agreement with the experiment is quite interesting. At 14 eV, the present Sherman functions display a comparable agreement with the experiment as that between RCCC and the experiment. In Figure 3, we compare our Sherman functions at 7 and 7.5 eV against those of the RCCC calculations with discrepancies to note. These slight differences are the positions of the maxima and the values of the minima of the Sherman function at the two

energies, which were also observed at other impact energies. No experimental data are available for these two energies.

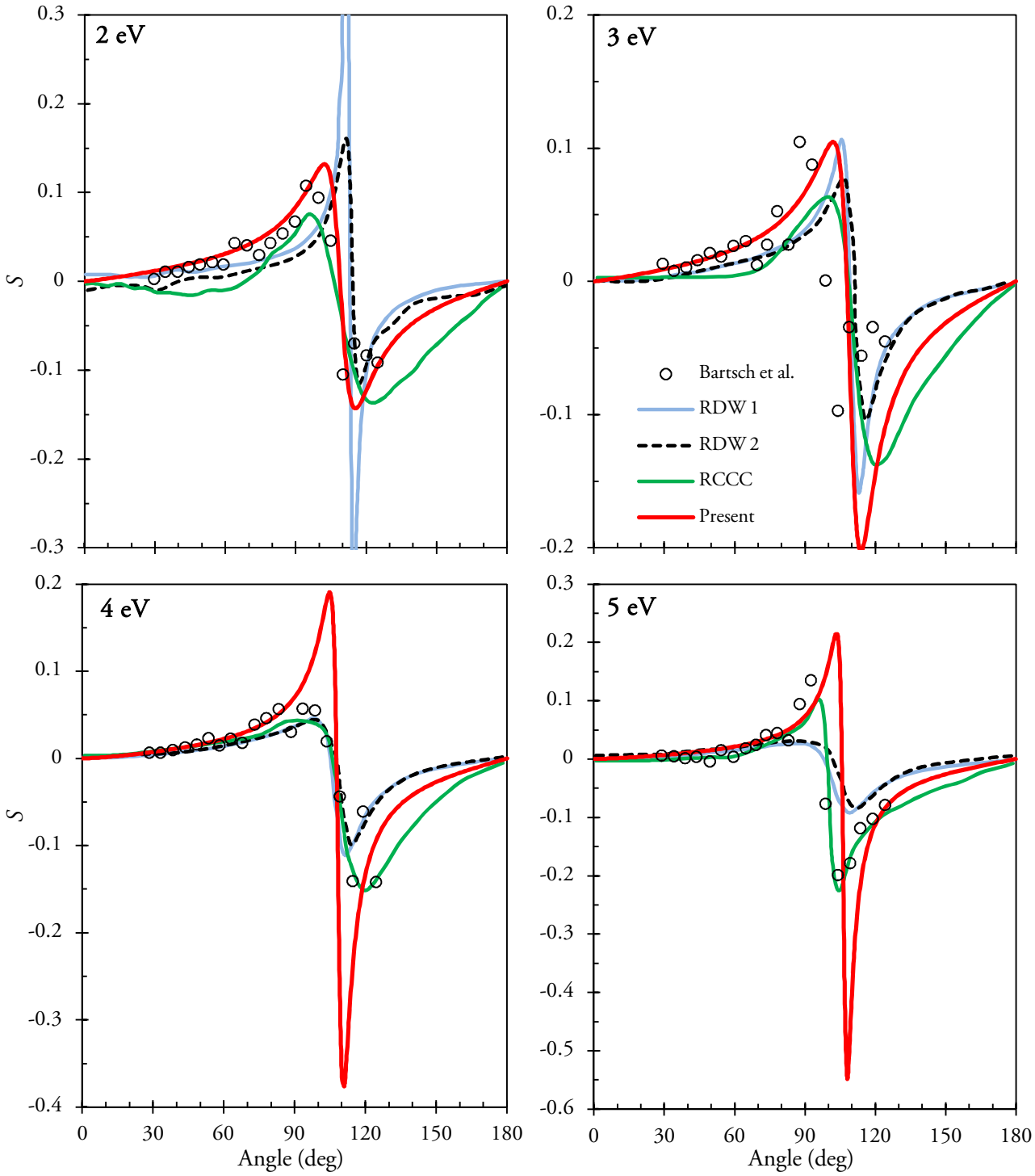


Figure 1. Sherman function for electron scattering from zinc at 2, 3, 4 and 5 eV: the legend in the figure describes markers for the present work; experiment: Bartsch et al. [1]; other theoretical: 66-state RCCC [5], RDW 1 [2] and RDW 2 [4].

Finally, a three-dimensional (3D) graph of the present Sherman function versus the impact energy and scattering angle for elastic e-Zn scattering is provided in Figure 4 to obtain a comprehensive view of the behavior of $S(\theta, E)$. The 3D presentation starts with positive values in the forward direction and negative values in the backward direction

alongside an inflection point around 110°. As impact energy rises the inner atomic shells increasingly affect the interaction, resulting in the movement of the inflection point and the development of secondary maxima and minima. In the case of Zn, a total of two minima in the angle are gradually being displayed before returning to a shallow minimum at high energies. The two minima correspond to the two fully occupied electronic shells $K(n = 1)$ and $L(n = 2)$.

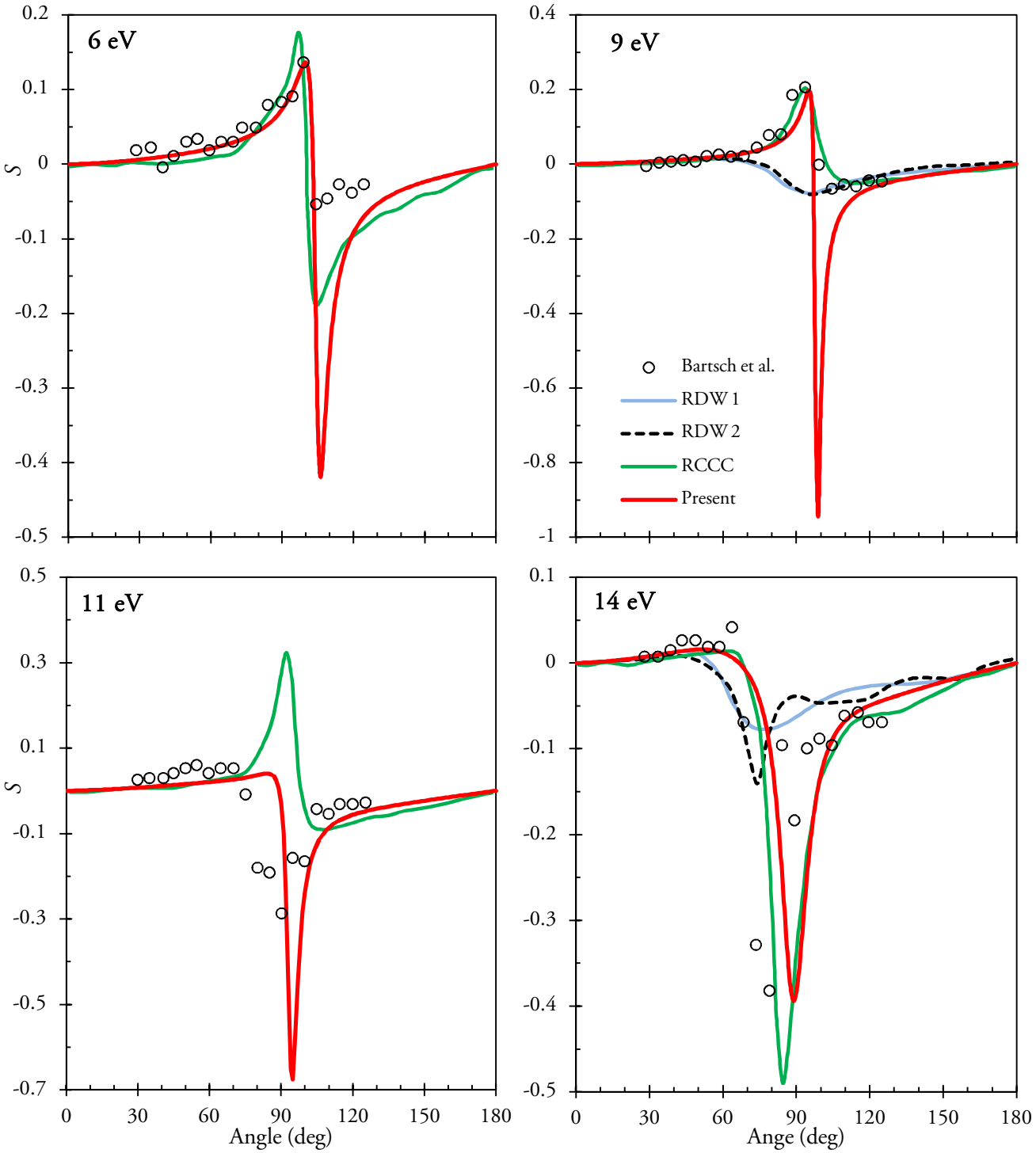


Figure 2. Same as for Figure 1 but at 6, 9, 11 and 14 eV projectile energies, Bartsch et al. [1].

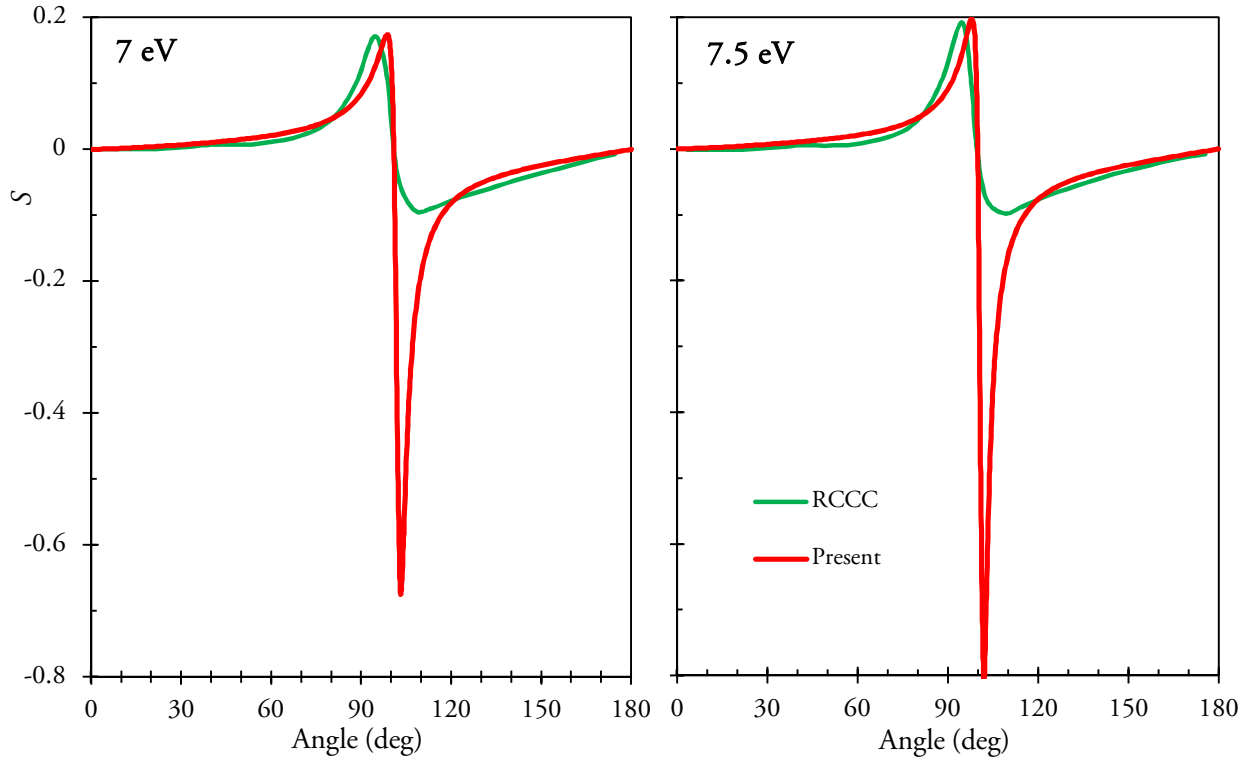


Figure 3. Comparisons between present Sherman function values at 7 and 7.5 eV with those of 66-state RCCC [5] calculations.

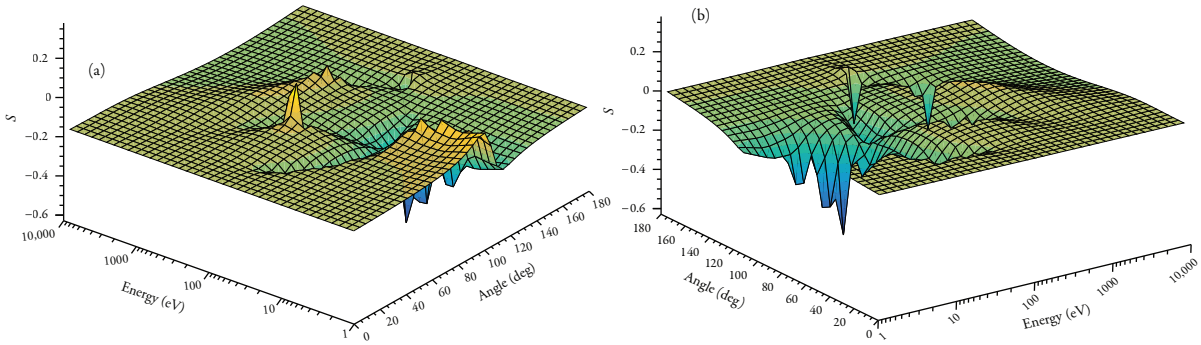


Figure 4. A three-dimensional view of the Sherman function for electron scattering from zinc: (**a**) top view, (**b**) bottom view.

3.2. Cadmium

The measurements of Bartcsh et al. [1] are the only experimental data on spin asymmetry for elastic electron scattering off cadmium. We compare our Sherman functions, in Figures 5–7, with the available experimental data and all other theoretical works, which include the 55-state RCCC method and the relativistic optical potential (ROP) calculations of Berrington et al. [7] and the relativistic polarized orbital approach of Szmytkowski and Sienkiewicz [4]. Very good agreement with the experiment is observed for energies up to 2 eV, particularly in the forward direction. The agreement at these energies with RCCC results is at least qualitative, if not very good. For energies above 2 eV, and approaching the threshold for the $(5s5p)\ ^3P_{0,1,2}$ excited states and the $(5s5p^2)\ ^3D_{3/2,5/2}$ negative ion state, our agreement with the experiment is rather spotty. Setting aside the accurate RCCC predictions, the other single-channel calculations (RPO and ROP) generally agree with ours but not with the experiment at these energies either.

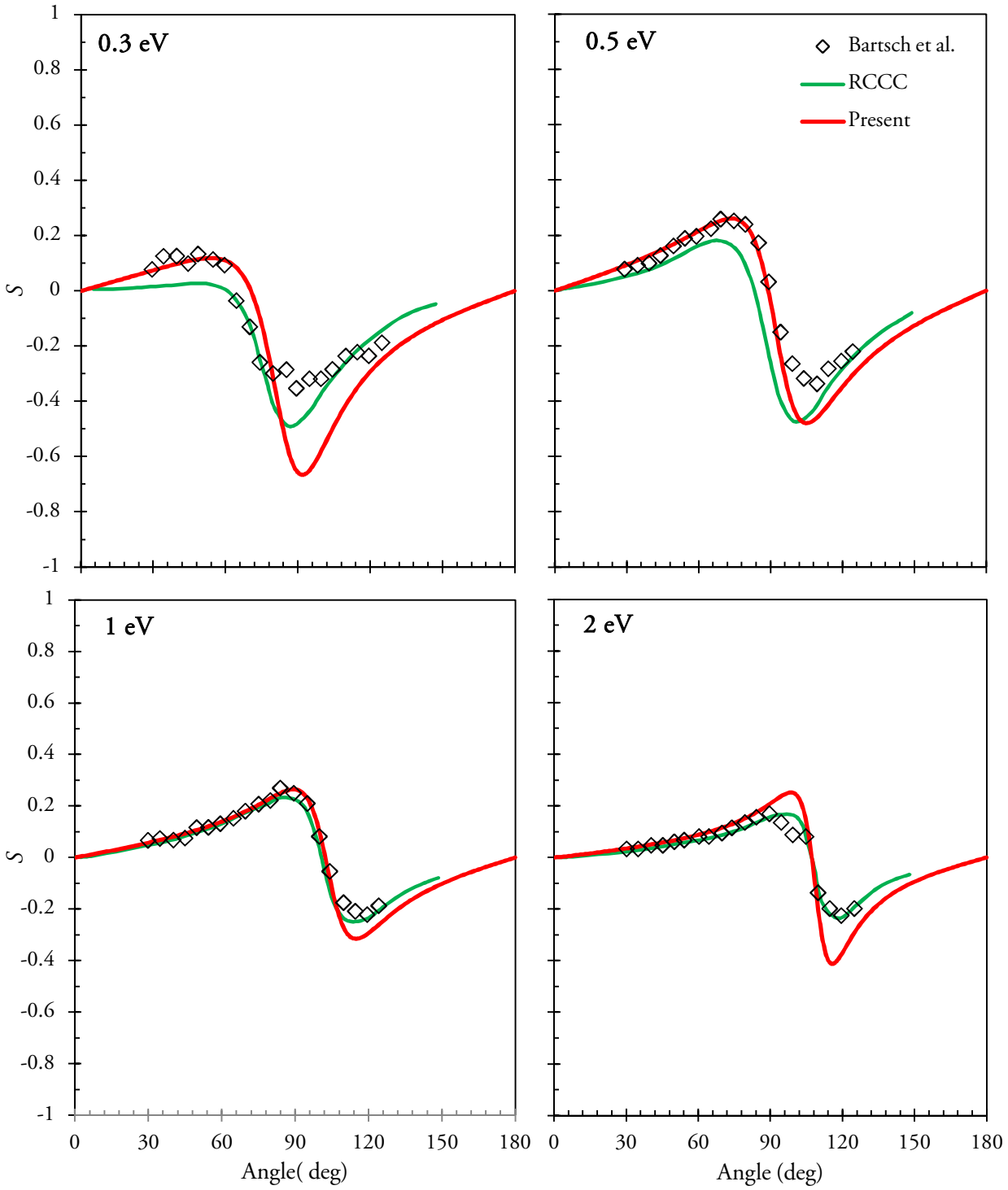


Figure 5. Sherman function for electron scattering from cadmium at 0.3, 0.5, 1 and 2 eV: the legend in the figure describes markers for the present work; experiment: Bartsch et al. [1]; other theoretical: 55-state RCCC [7] calculations.

Our Sherman functions at 5 and 6 eV impact energies show an excellent agreement with the experiment in the forward direction, while disagreeing by a few degrees on the location of the maximum with the RCCC Sherman functions. At both energies, ROP results show considerable discrepancies with the experiment. Our Sherman function at 9 eV displays a remarkable agreement with the experiment, while RCCC is the only other calculation agreeing with the experiment at this energy. In Figure 8, we present our Sherman function values at 110° as a function of energy in comparison with the experiment and the

theoretical results from the RCCC and ROP approaches. The swift rise in Sherman function values at 110° between 3.7 and 4.2 eV is due to the formation of negative ion resonances and excited states in this energy interval (discussed in Ref. [45]). Our Sherman function at 110° shows a displaced ascent while following the experiment and RCCC through a downward bias. The overall energy behavior of our results is good in spite of the single-channel nature of the approach.

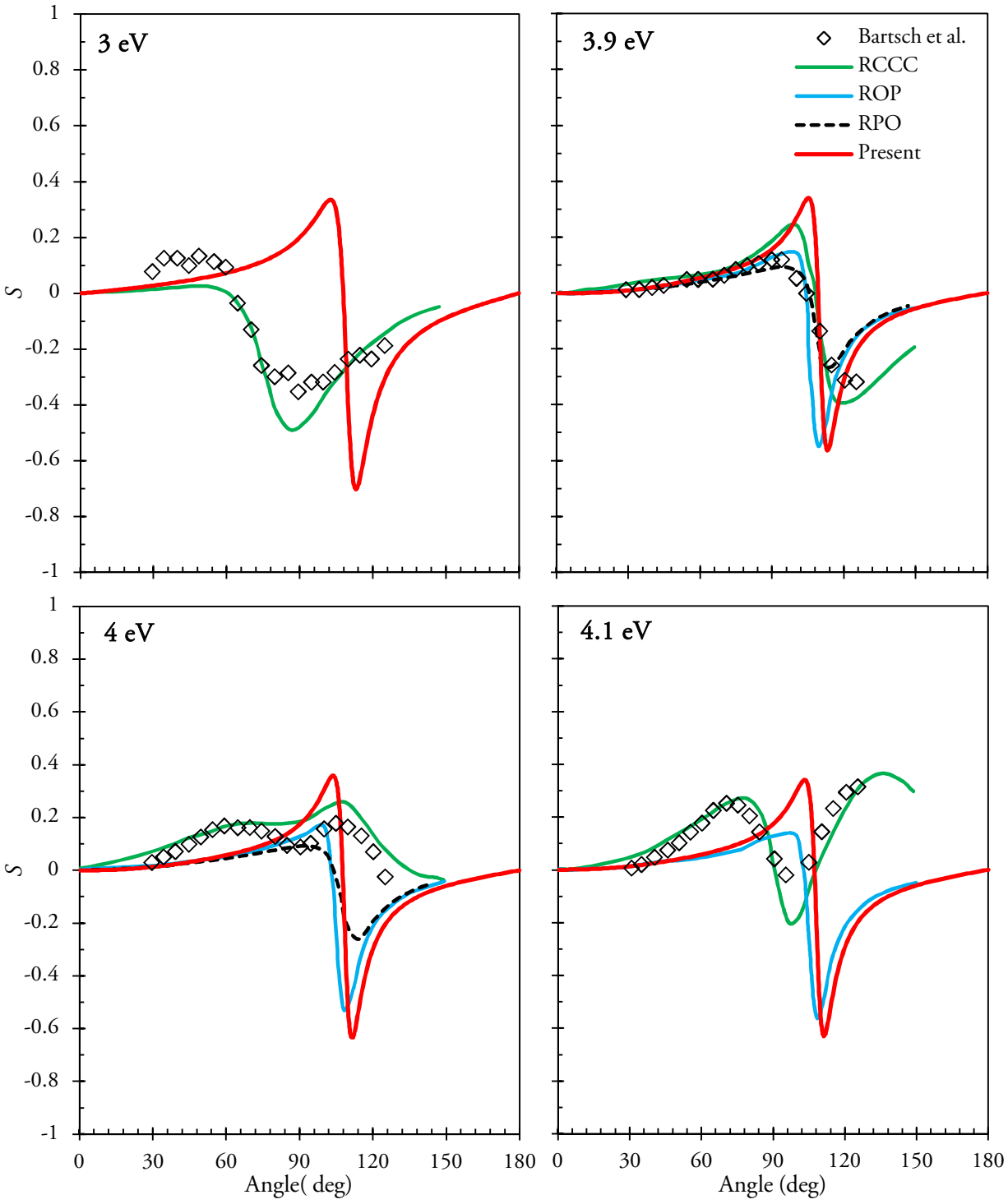


Figure 6. Same as for Figure 5 but at 3, 3.9, 4 and 4.1 eV projectile energies, Bartsch et al. [1]. Additional theoretical works are ROP [7] and RPO [4] calculations.

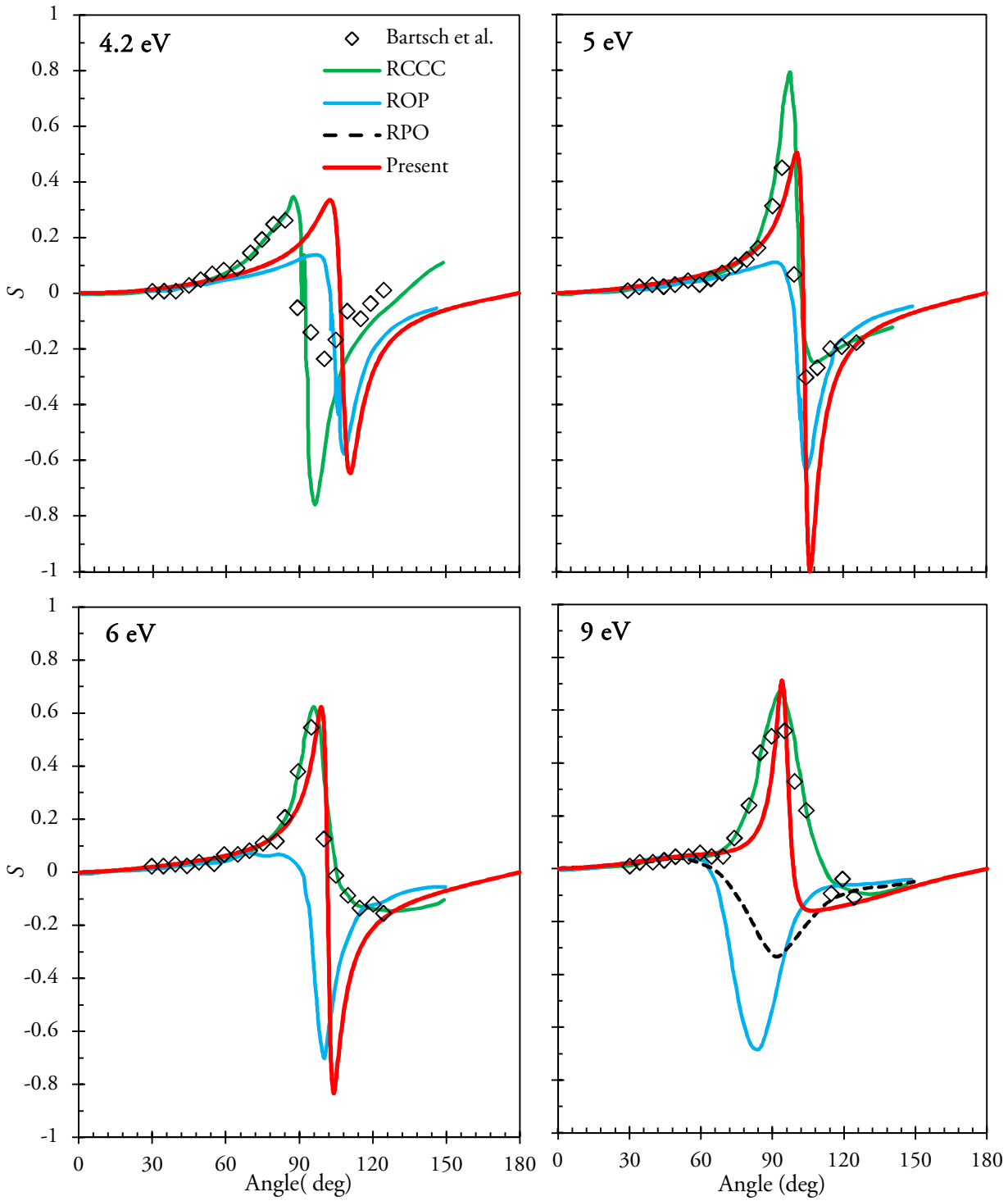


Figure 7. Same as for Figure 6 but at 4.2, 5, 6 and 9 eV projectile energies, Bartsch et al. [1].

The 3D graph of the Sherman function against the impact energy and scattering angle for elastic e-Cd scattering is presented in Figure 9. Here again we see the evolution of $S(\theta)$ as energy increases and the structure of the inner atomic shells is felt by the projectiles. Unfortunately, no experimental or theoretical data exist at energies above 9 eV. Our calculations provide the only data, which probes in depth the spin–orbit interaction effects at medium and high energies. The overall behavior is similar to that of zinc, but displaying the development of three minima in the angular distribution, reflecting the now three fully occupied electronic shells, i.e., $K(n = 1)$, $L(n = 2)$, and $M(n = 3)$.

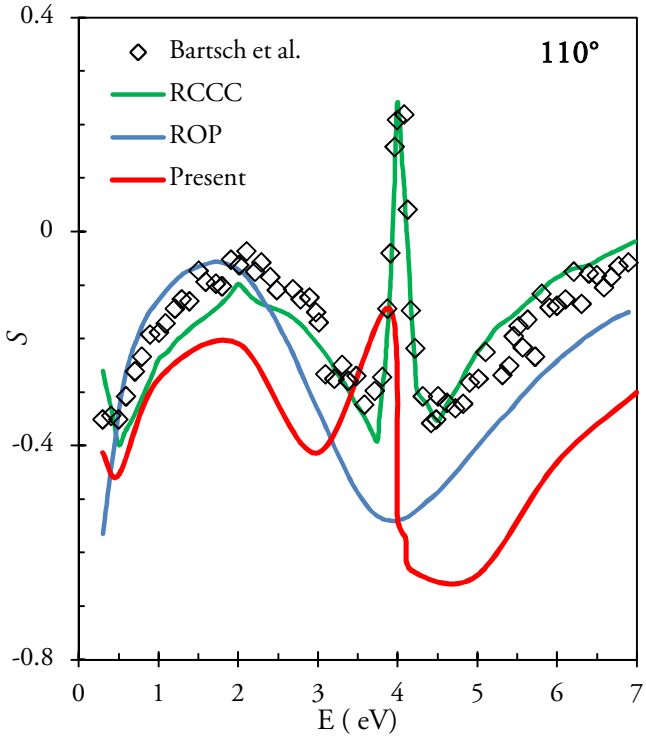


Figure 8. Sherman function for electron scattering from cadmium at a scattering angle of 110° versus impact energy. The legend in the figure describes markers for the present work; experiment: Bartsch et al. [1]; other theoretical: 55-state RCCC [7] and ROP [7] calculations.

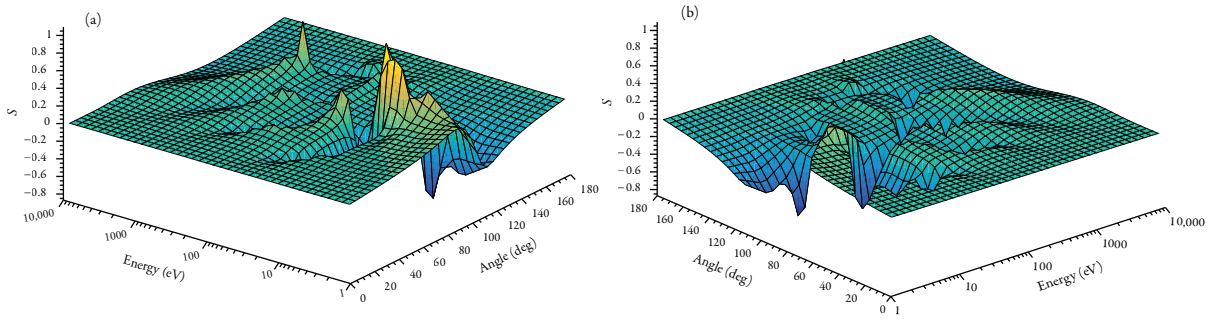


Figure 9. A three-dimensional view of the Sherman function for electron scattering from cadmium: (**a**) top view, (**b**) bottom view.

3.3. Mercury

As mentioned in the introduction for mercury there is a plethora of spin asymmetry measurements, some of them going back to 1956. The work of Düweke et al. [15] is limited to energies below 4 eV, and that of Dümmler et al. [22] is limited to less than 2 eV. Above 6 eV impact energy, we have the works of Kaussen et al. [21] (6–24, and 180 eV), Hanne et al. [17] (8, 10, 12, and 18 eV), and Deichsel et al. [11] (3.5, 7, 23, and 45 eV). At intermediate energies, there exist the works of Eitel et al. [12] (18.3, 25, 30, 50, and 180 eV) and that of Berger and Kessler [20] (25, 35, 50, and 150 eV). Finally, at the upper range of impact energies we have the works of Jost and Kessler [10] (180 to 340 eV) and Eitel et al. [12] (100–2000 eV). Thus we have experimental data in a wide range of impact energies to compare our theoretical predictions with.

In Figures 10–20, we present a detailed comparison of our Sherman functions for mercury, from 1 eV to 500 eV, with experimental and select theoretical data. The theoretical works in the comparisons include the 66-state RCCC calculations of Bostock et al. [5], the R-matrix calculations of Bartschat et al. [26], the generalized density-functional calculations (GDF) of Haberland and Fritsche [27], the relativistic distorted-wave method (RDW) of McEachran and Stauffer [28], and the optical potential (OP) calculations of Haque et al [32].

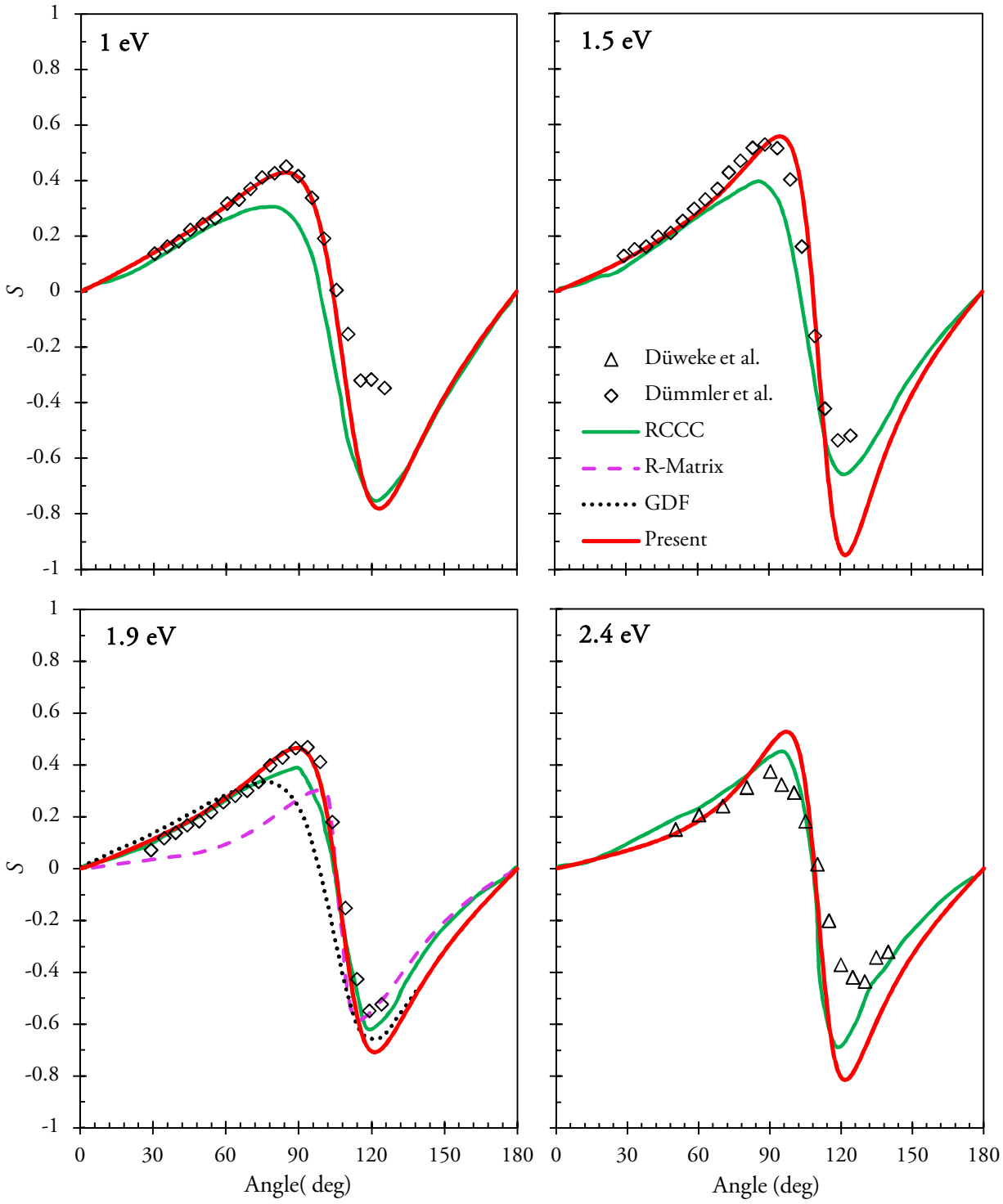


Figure 10. Sherman function for electron scattering from mercury at 1, 1.5, 1.9 and 2.4 eV: the legend in the figure describes markers for the present work; experiment: Düweke et al. [15] and Dümmler et al. [22]; other theoretical: 66-state RCCC [5], R-matrix [26] and GDF [27].

In Figure 10, our Sherman functions display a very good agreement with the measurements of Dümmler et al. [22] at energies of 1, 1.5 and 1.9 eV. In the same figure and at energy 2.4 eV, the RCCC values and our Sherman functions, while in mutual agreement, only exhibit partial agreement with the experimental data of Düweke et al [15]. At energies of 3.5, 3.9, 6 and 7 eV, our Sherman functions agree with the experiment quite well, mainly in the forward direction, as shown in Figure 11.

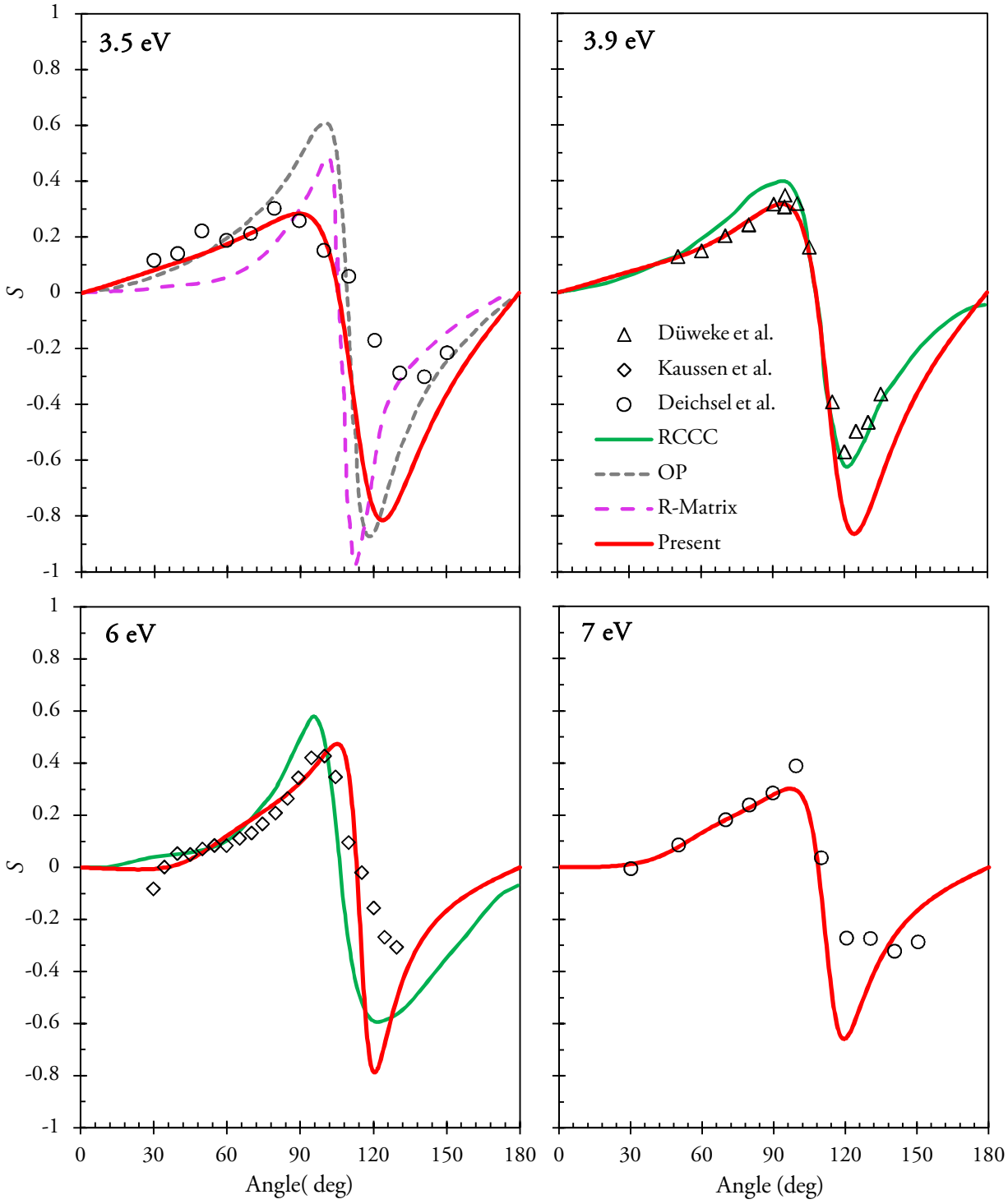


Figure 11. Same as for Figure 10 but at 3.5, 3.9, 6 and 7 eV projectile energies, Düweke et al [15]. Additional experiments: Kaussen et al. [21] and Deichsel et al. [11]; additional theoretical: OP [32].

In Figure 12, our values agree with the measurements of Hanne et al. [17] at impact energies of 8 and 10 eV, while throughout the angular range, they disagree with the OP predictions at those energies. In the same figure, our data show a considerably good agreement with the experiment of Kaussen et al. [21] and RCCC values at 9 and 11 eV.

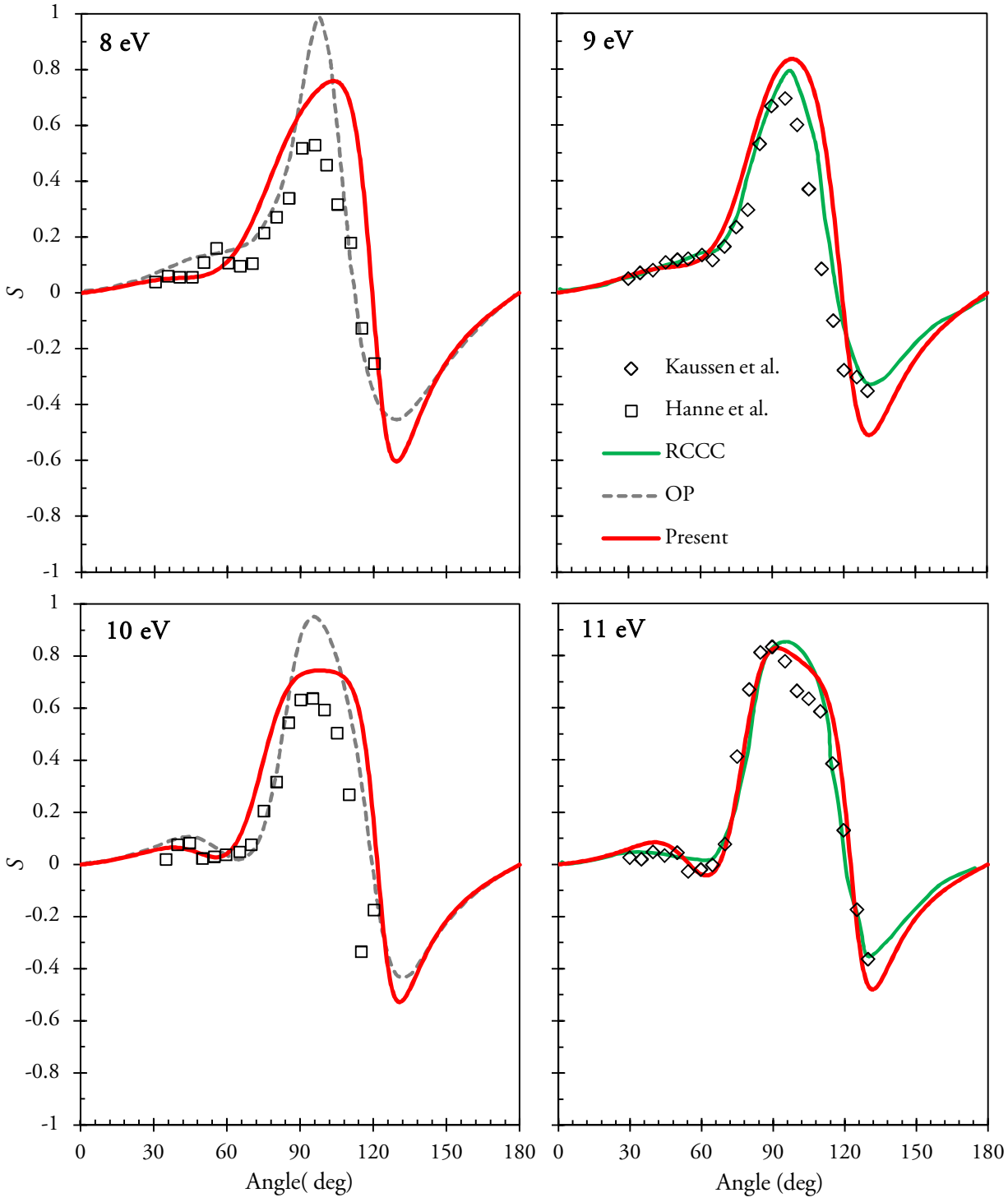


Figure 12. Same as for Figure 11 but at 8, 9, 10 and 11 eV projectile energies, Kaussen et al. [21]. Additional experiment is Hanne et al [17].

We observe an excellent agreement, in Figure 13, with the experiment at 12 eV. Very good agreement with the experiment is also on display at 12.2 and 14 eV, while not quite reaching the measured values at the two minima of $S(\theta)$. The agreement with the experi-

ment at 15 eV is improved in the forward direction, while notable disagreement is observed with the values of the OP calculations.

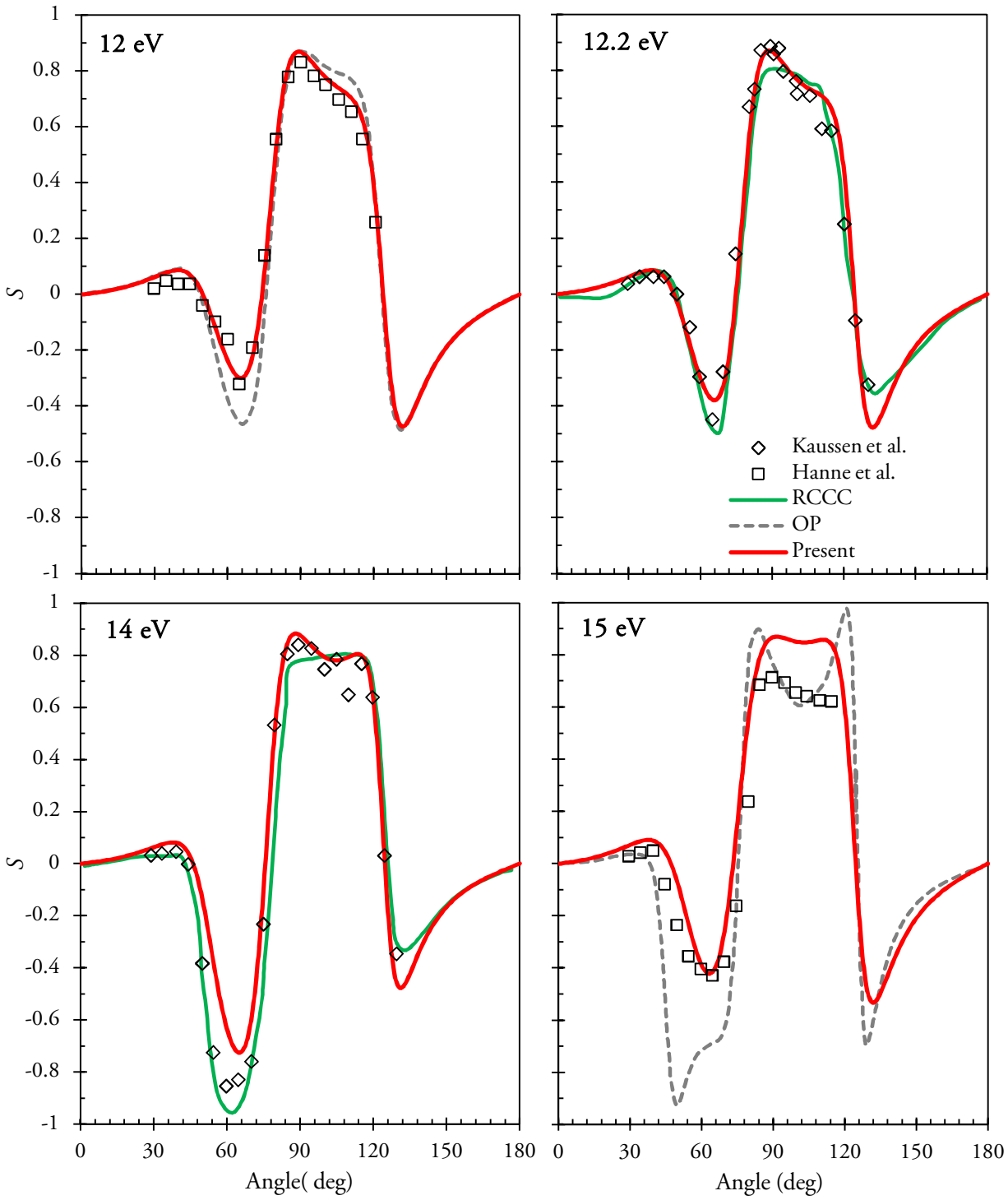


Figure 13. Same as for Figure 12 but at 12, 12.2, 14 and 15 eV projectile energies, Kaussen et al. [21], Hanne et al [17].

Our Sherman functions, in Figure 14, show good agreement with the experimental results of Kaussen et al. [21] at 17 and 24 eV. However, considerable disagreement is observed with the measurements of Hanne et al. [17] at 18 eV and Deichsel et al. [11] at 23 eV. A remarkable change in the shape of the *S* function is seen at energies above 10 eV, with additional peaks and dips gradually appearing. There are no other theoretical data to compare with at these energies.

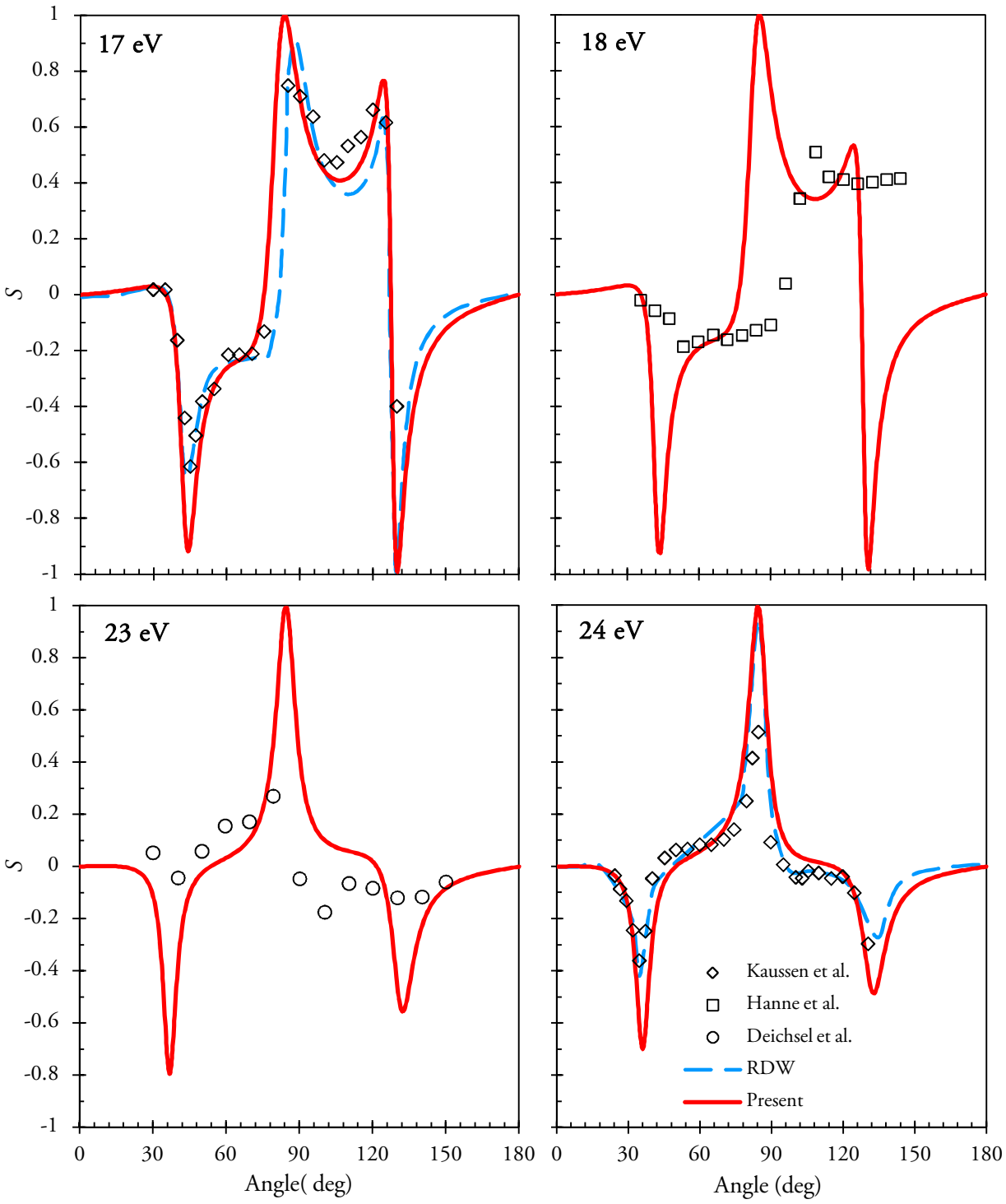


Figure 14. Same as for Figures 11 and 13 but at 17, 18, 23 and 24 eV projectile energies, Kaussen et al. [21], Hanne et al [17], Deichsel et al. [11]. Additional theoretical work is RDW [28].

For energies above 23 eV it is clear that the theory accurately predicts the experimentally confirmed physics of electron polarization during elastic scattering from mercury. In Figure 15, the present results display good agreement with experimental data while slightly disagreeing with those of OP on the positions of the first minimum and the maximum at 25 eV impact energy. The RDW results follow our values nicely.

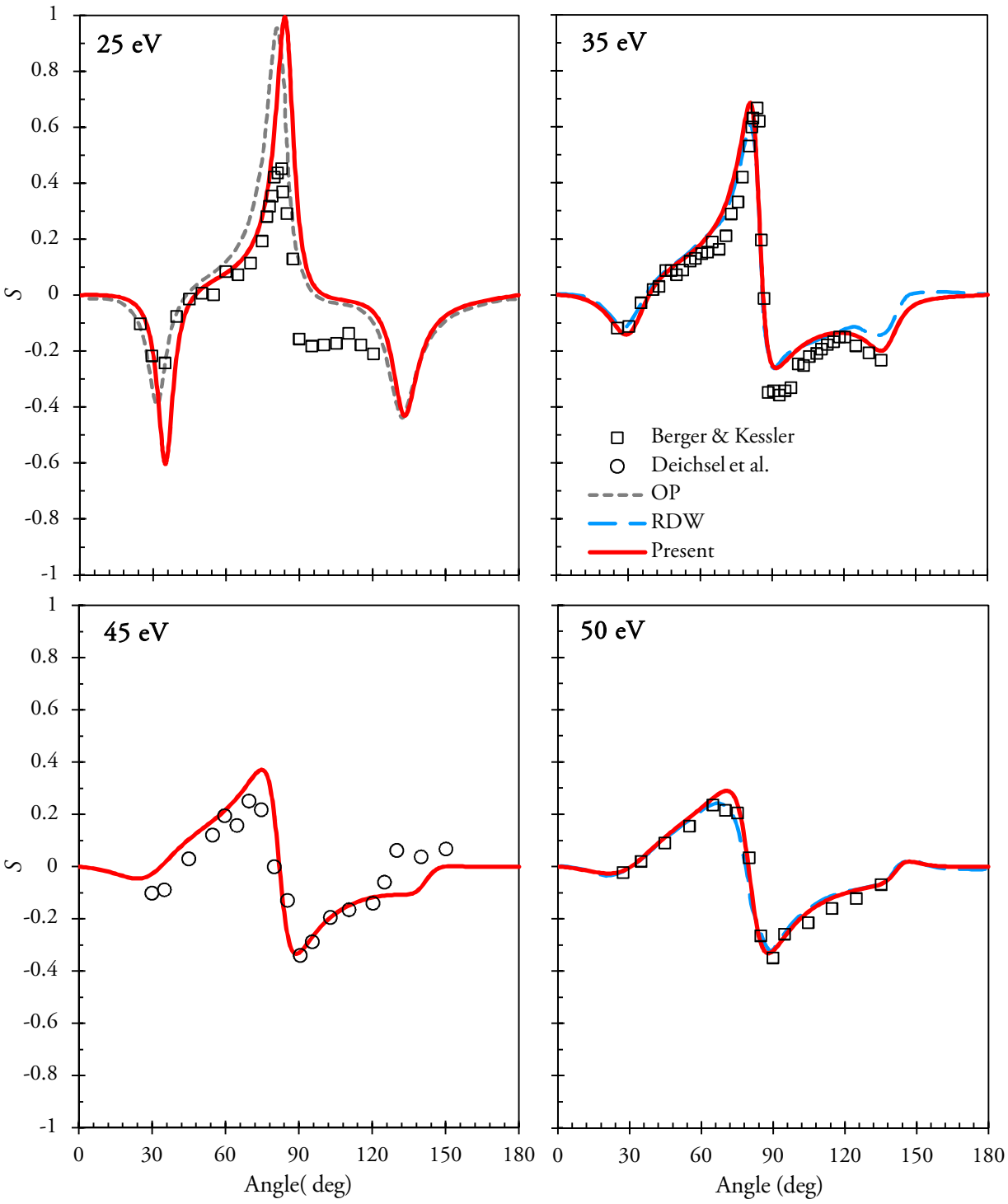


Figure 15. Same as for Figures 11 and 14 but at 25, 35, 45 and 50 eV projectile energies, Deichsel et al. [11]. Additional experiment is Berger and Kessler [20].

Present Sherman functions, in Figure 16, display excellent agreement with experimental data. Our values differ slightly from those of RDW at 150 eV only in the backward direction, whereas visible differences are on display between our Sherman functions and those of the OP calculations at 100, 170 and 180 eV in Figure 16.

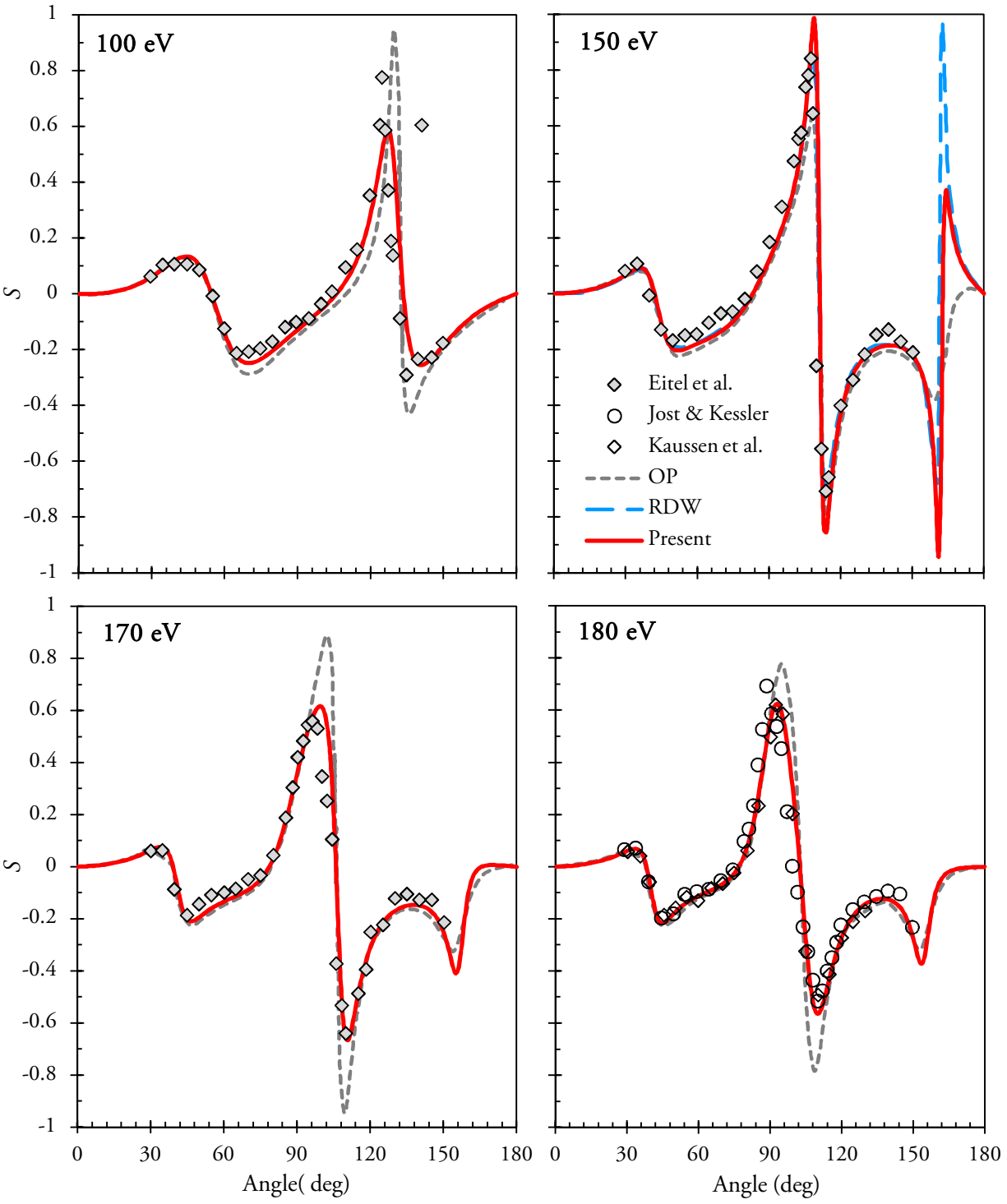


Figure 16. Same as for Figures 15 but at 100, 150, 170 and 180 eV projectile energies, Kaussen et al. [21]. Additional experiments are Jost and Kessler [10] and Eitel et al. [12].

At higher impact energies, our results are in excellent agreement with the available experimental data, as shown in Figures 17–19. No other calculations exist above 230 eV, other than an OP one at 500 eV, which agrees very well with ours.

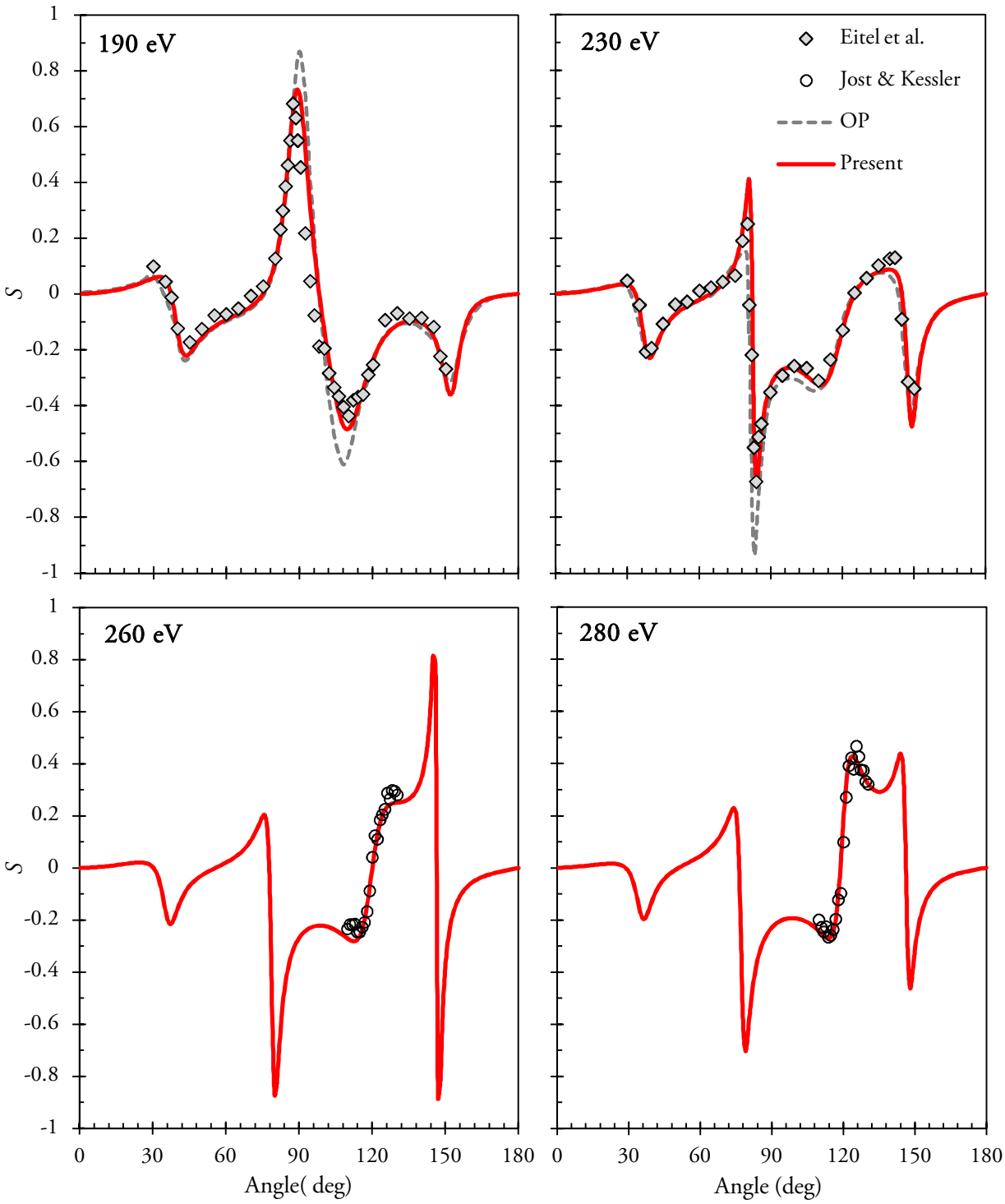


Figure 17. Same as for Figure 16 but at 190, 230, 260 and 280 eV projectile energies, Jost and Kessler [10] and Eitel et al. [12].

In Figure 20, we compare our Sherman function values at 50° with measurements of Albert et al. [16], at 60° with those of Dümmler et al. [22], and at 75° and 90° with the experimental results of Hanne et al. [17], Jost and Kessler [10], Mölenkamp et al. [19] and Eitel and Kessler [13] for various energy intervals. Overall the agreement with the experimental data is very good.

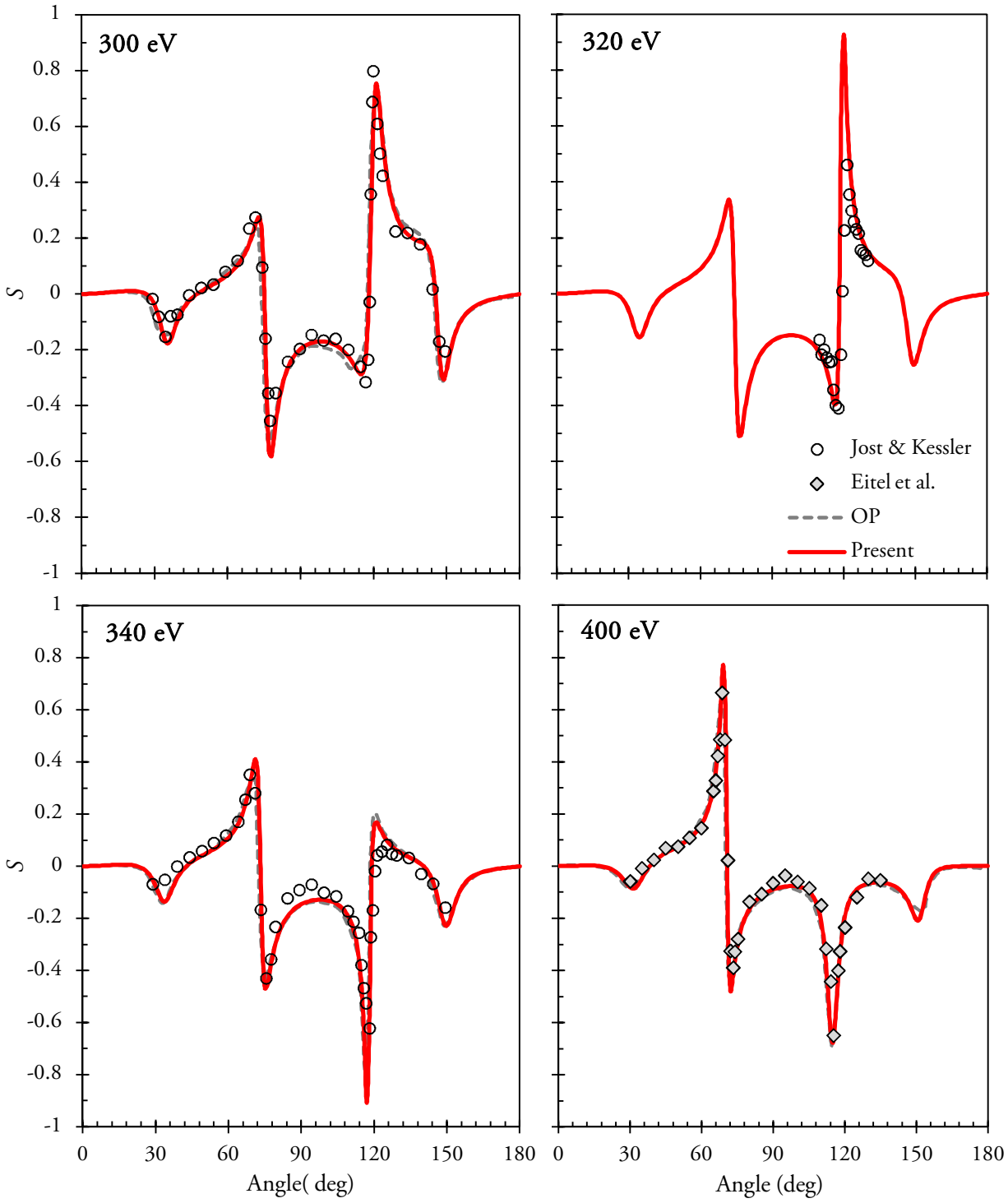


Figure 18. Same as for Figure 17 but at 300, 320, 340 and 400 eV projectile energies, Jost and Kessler [10] and Eitel et al. [12].

Further comparisons with the experimental data of Mölenkamp et al. [19] and Eitel et al. [12] at 90° are displayed in Figure 21 for energies up to 2600 eV, exhibiting excellent agreement. In the same figure, our Sherman function values at 117° and 135° show a strong disagreement in the energy interval of 4–6 eV with measurements of Düweke et al. [15] and Albert et al. [16], respectively. This is not very surprising, as our Sherman functions did not display good agreements with experimental data in the backward direction at those energies (see Figure 11).

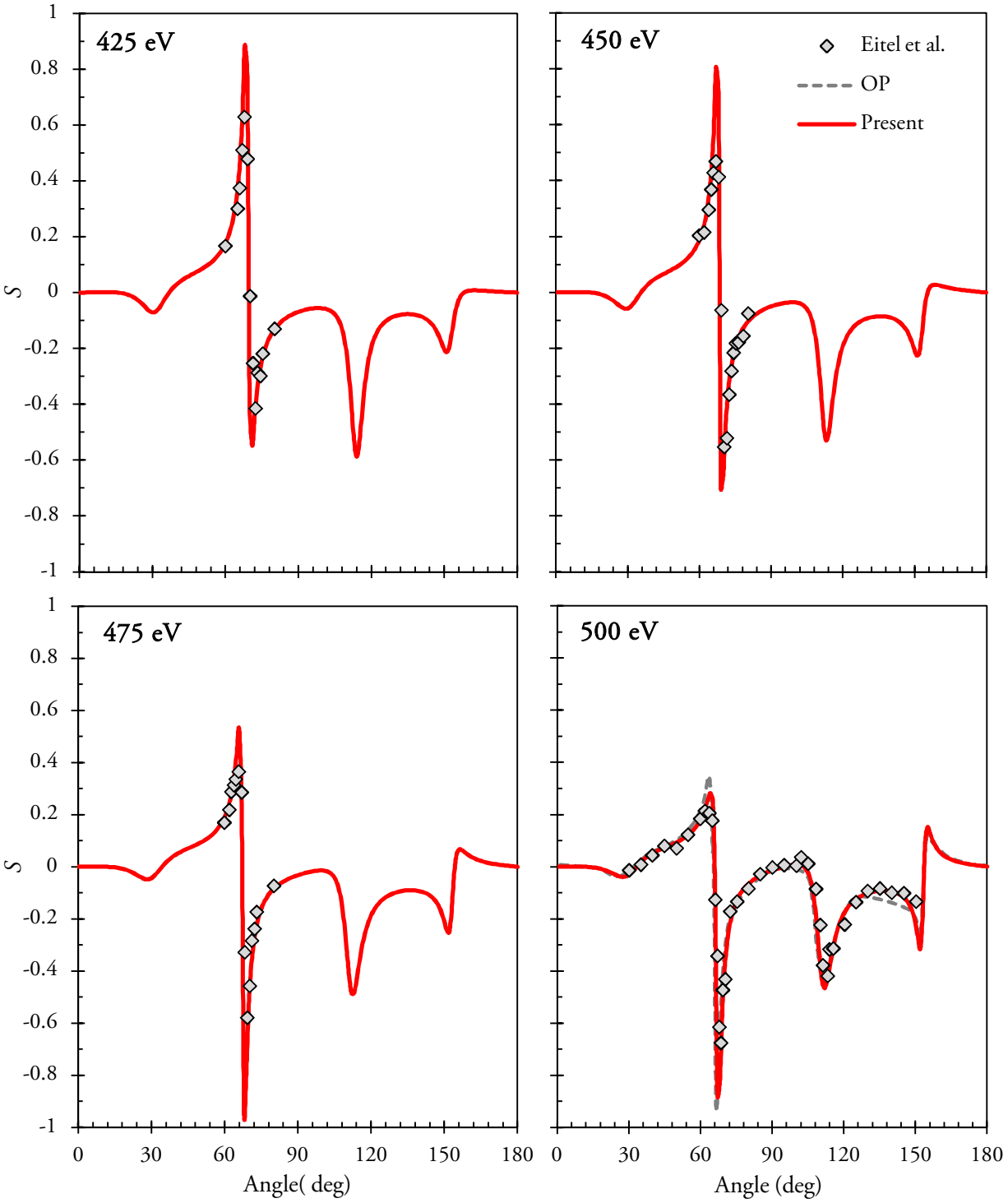


Figure 19. Same as for Figure 18 but at 425, 450, 475 and 500 eV projectile energies, Eitel et al. [12].

Finally, Figure 22 displays the 3D graph of the Sherman function against the impact energy and scattering angle for elastic e-Hg scattering to provide a global perspective. Similar to the cases of zinc and cadmium, as impact energy increases, the scattered electrons reach deeper into the atomic core of the target atom, probing its shell structure. In the case of mercury the initial one minimum, at low energies, evolves into eventually four minima, before returning to a single shallow one at very high energies. The number of the developing minima reflects the gradual probing, with increasing energy, of all the *fully* occupied electronic shells in the target atom, in the case of mercury being K (n=1), L (n=2), $M(n = 3)$, and $N(n = 4)$. A useful discussion on the order of the filling of atomic orbitals with an

increasing atomic number, including the physical collapse of, e.g., the $4f$ subshell when fully occupied, is given by Fano et al [46].

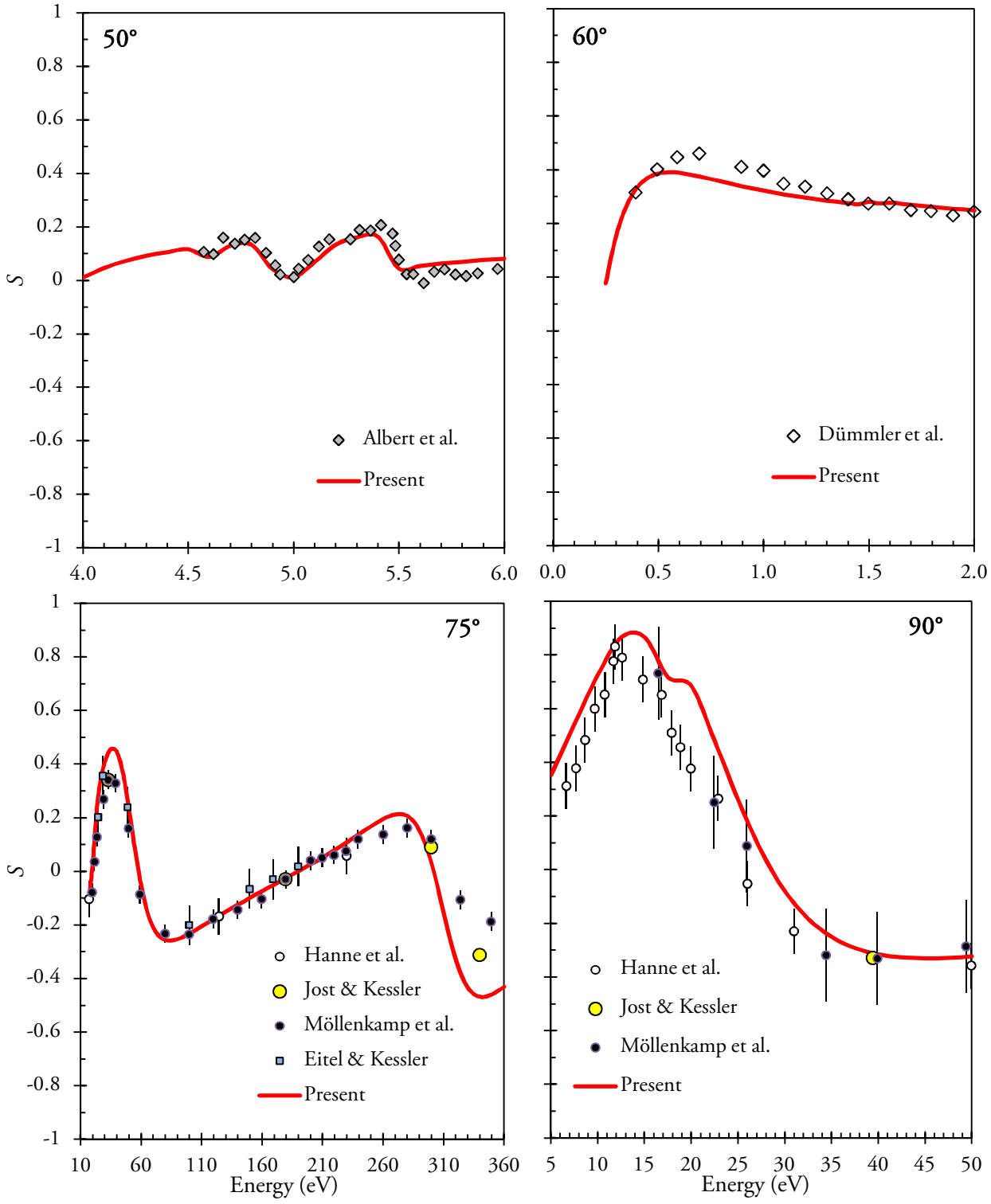


Figure 20. Sherman function for electron scattering from mercury at 50°, 60°, 75° and 90° scattering angles. The legend in the figure describes markers for the present work; experiment: Albert et al. [16], Dümmler et al. [22], Hanne et al. [17], Jost and Kessler [10], Mölenkamp et al. [19] and Eitel and Kessler [13].

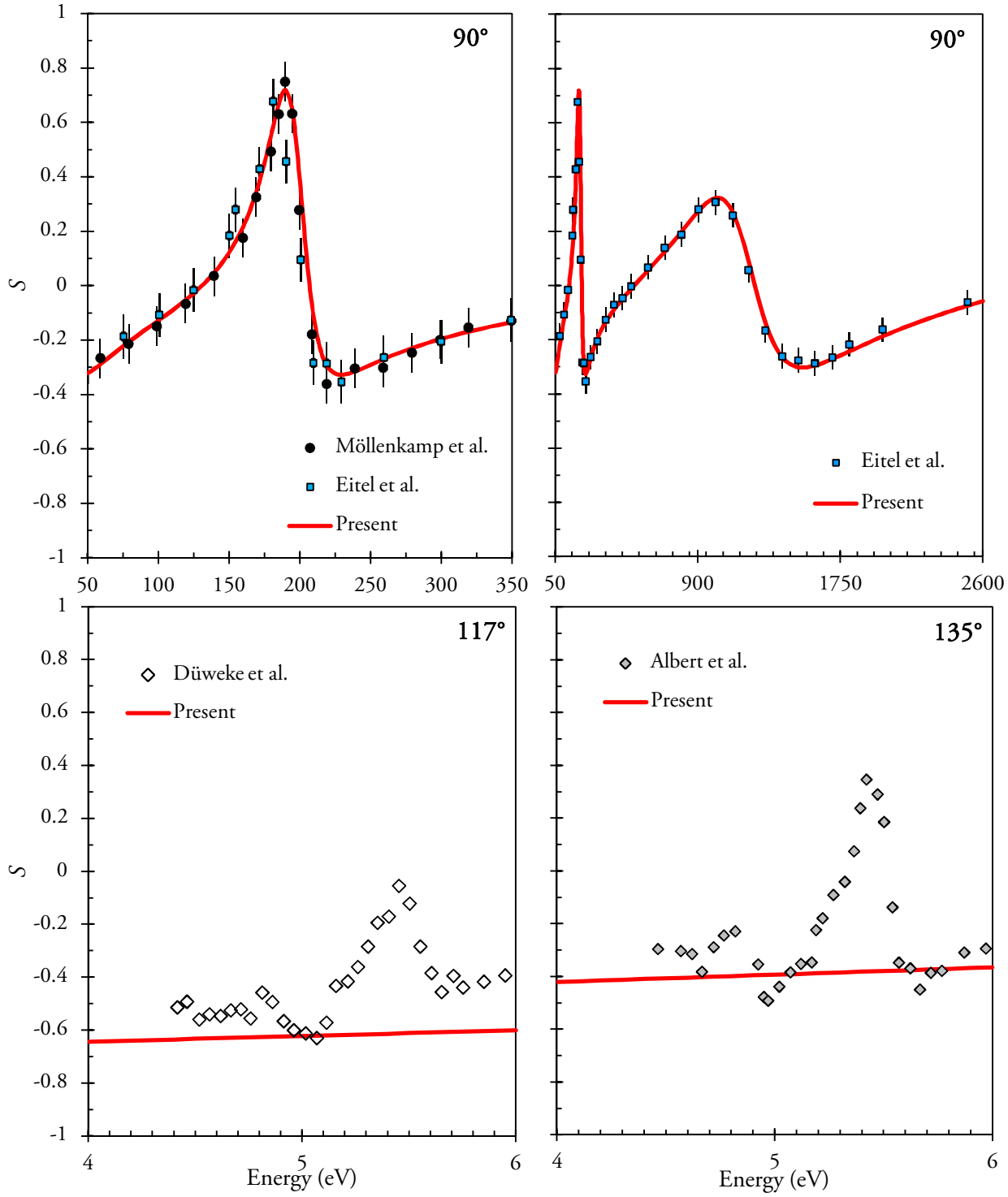


Figure 21. Same as for Figure 20 but at 90°, 117° and 135° scattering angles, Mölenkamp et al. [19], Eitel et al. [13], Albert et al. [16]. Additional experiment is Düweke et al. [15].

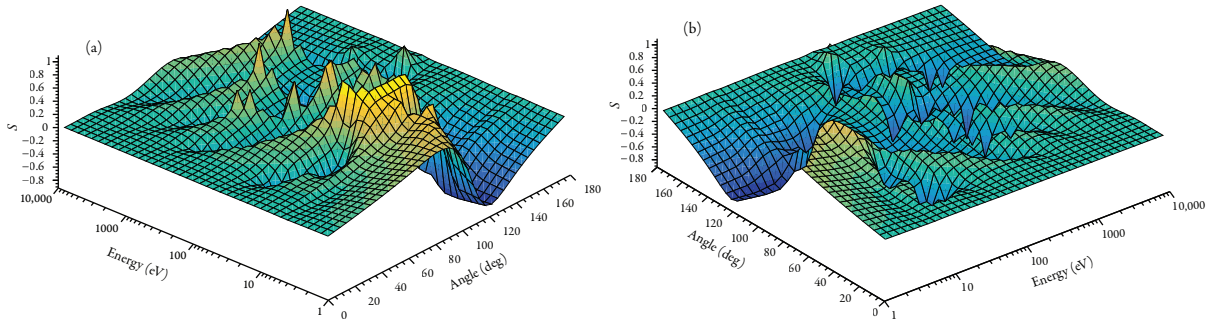


Figure 22. A three-dimensional view of the Sherman function for electron scattering from mercury: (**a**) top view, (**b**) bottom view.

4. Conclusions

In this work we have extended our previous work using a self-consistent relativistic calculation of the spin-polarization of elastically scattered electrons from Zn, Cd, and Hg, thus completing these types of study for all quasi-two-electron atoms. The 3D graphs of $S(\theta, E)$, extending to 10 keV incident energy, provide a vivid illustration of how elastically scattered electrons with increasing incident energy, probe deeper and deeper into the atomic structure, directly displaying the presence of the $K(n = 1)$, $L(n = 2)$, $M(n = 3)$, and $N(n = 4)$ atomic shells when they become fully occupied. The Dirac–Slater central target potential was supplemented with an exchange potential and a target-polarization term, which contains the only adjustable parameter of this approach, i.e., the cutoff radius of the polarization potential. We view the overall agreement with all the available experimental data and sophisticated calculations as quite satisfactory. The present comprehensive data aim to serve as a reliable reference basis, covering an extensive energy range, for future investigations.

Supplementary Materials: The following supporting information can be downloaded at: https://www.mdpi.com/article/10.3390/atoms14070057/s1.

Author Contributions: Conceptualization, M.A. and C.E.T.; methodology, M.A. and C.E.T.; software, M.A. and C.E.T.; validation, M.A. and C.E.T.; formal analysis, M.A. and C.E.T.; data curation, M.A. and C.E.T.; writing—original draft preparation, M.A.; writing—review and editing, M.A. and C.E.T.; visualization, M.A.; supervision, M.A. and C.E.T. All authors have read and agreed to the published version of the manuscript.

Funding: This research received no external funding.

Data Availability Statement: The original contributions presented in this study are included in the article/Supplementary Material. Further inquiries can be directed to the corresponding author.

Conflicts of Interest: The authors declare no conflicts of interest.

References

1. Bartsch, M.; Geesmann, H.; Hanne, G.F.; Kessler, J. Asymmetric scattering of polarized electrons from atoms with closed and open shells. *J. Phys. B At. Mol. Opt. Phys.* **1992**, *25*, 1511. [CrossRef]
2. McEachran, R.P.; Stauffer, A.D. Spin polarization of electrons elastically scattered from cadmium and zinc. *J. Phys. B At. Mol. Opt. Phys.* **1992**, *25*, 1527. [CrossRef]
3. Kumar, P.; Jain, A.K.; Tripathi, A.N.; Nahar, S.N. Spin-polarization parameters and cross sections for electron scattering from zinc and lead atoms. *Phys. Rev. A* **1994**, *49*, 899–907. [CrossRef] [PubMed]
4. Szmytkowski, R.; Sienkiewicz, J.E. Spin polarization of slow electrons elastically scattered from mercury, cadmium and zinc atoms. *J. Phys. B At. Mol. Opt. Phys.* **1994**, *27*, 555. [CrossRef]
5. Bostock, C.J.; Fursa, D.V.; Bray, I. Relativistic convergent close-coupling method calculation of the spin polarization of electrons scattered elastically from zinc and mercury. *Phys. Rev. A* **2012**, *85*, 062707. [CrossRef]

6. Nahar, S.N. Cross sections and spin polarizations for $e^{\pm}$ scattering from cadmium. *Phys. Rev. A* **1991**, *43*, 2223–2236. [CrossRef] [PubMed]
7. Berrington, M.J.; Bostock, C.J.; Fursa, D.V.; Bray, I.; McEachran, R.P.; Stauffer, A.D. Calculations of electron scattering from cadmium. *Phys. Rev. A* **2012**, *85*, 042708. [CrossRef]
8. Haque, M.M.; Haque, A.K.; Uddin, M.A.; Maaza, M.; Patoary, M.A.R.; Basak, A.K.; Saha, B.C. Chapter One—Elastic scattering of e± by Cd, Hg, and Pb atoms at 1 $eV \leq Ei \leq 1$ GeV. In *Advances in Quantum Chemistry*; Academic Press: Cambridge, MA, USA, 2021; Volume 84, pp. 1–72. [CrossRef]
9. Deichsel, H. Herstellung und Nachweis polarisierter Elektronenstrahlen durch zweimalige Streuung von Glühelektronen kleiner Energie (1–2 keV) an Hg-Atomstrahlen. *Z. Phys.* **1961**, *164*, 156–165. [CrossRef]
10. Jost, K.; Kessler, J. Zur Polarisation langsamer Elektronen durch Streuung an Quecksilber zwischen 180 und 1700 eV. *Z. Phys.* **1966**, *195*, 1–12. [CrossRef]
11. Deichsel, H.; Reichert, E.; Steidl, H. Elektronenpolarisation im Energiebereich unterhalb 50 eV durch Streuung an freien Hg-Atomen. *Z. Phys.* **1966**, *189*, 212–216. [CrossRef]
12. Eitel, W.; Jost, K.; Kessler, J. Polarization of Slow Electrons by Hg and Range of Applicability of the Relativistic Hartree Potential. *Phys. Rev.* **1967**, *159*, 47–49. [CrossRef]
13. Eitel, W.; Kessler, J. Spinpolarisation und differentielle Wirkungsquerschnitte bei der inelastischen Elektron-Atom-Streuung. *Z. Phys. A Hadron. Nucl.* **1971**, *241*, 355–368. [CrossRef]
14. Hanne, G.; Jost, K.; Kessler, J. Spinpolarisation und Winkelverteilung der Elektronen nach Anregung verschiedener Zustände des Hg-Atoms. *Z. Phys.* **1972**, *252*, 141–146. [CrossRef]
15. Düweke, M.; Kirchner, N.; Reichert, E.; Schön, S. Spin polarization in low-energy electron scattering from mercury. *J. Phys. B At. Mol. Phys.* **1976**, *9*, 1915. [CrossRef]
16. Albert, K.; Christian, C.; Heindorff, T.; Reichert, E.; Schön, S. Electron resonance scattering from mercury. *J. Phys. B At. Mol. Phys.* **1977**, *10*, 3733. [CrossRef]
17. Hanne, G.F.; Kollath, K.J.; Wubker, W. Electron spin polarisation resulting from elastic scattering of electrons by mercury atoms between 8 and 18 eV collision energy. *J. Phys. B At. Mol. Phys.* **1980**, *13*, L395. [CrossRef]
18. Berger, O.; Kessler, J.; Kollath, K.J.; Möllenkamp, R.; Wübker, W. "Triple" Scattering Experiment for Obtaining the Maximum Possible Information on Elastic Electron Scattering from Mercury. *Phys. Rev. Lett.* **1981**, *46*, 768–770. [CrossRef]
19. Möllenkamp, R.; Wübker, W.; Berger, O.; Jost, K.; Kessler, J. Elastic scattering of polarised electrons from mercury and xenon to obtain the complete information on the scattering process. *J. Phys. B At. Mol. Phys.* **1984**, *17*, 1107. [CrossRef]
20. Berger, O.; Kessler, J. Elastic scattering of polarised electrons from mercury and xenon. *J. Phys. B At. Mol. Phys.* **1986**, *19*, 3539. [CrossRef]
21. Kaussen, F.; Geesmann, H.; Hanne, G.F.; Kessler, J. Study of spin polarisation in elastic scattering of electrons from Hg, Tl, Pb and Bi atoms. *J. Phys. B At. Mol. Phys.* **1987**, *20*, 151. [CrossRef]
22. Dümmler, M.; Bartsch, M.; Geesmann, H.; Hanne, G.F.; Kessler, J. Low-energy data of the Sherman function of Hg, Tl and Pb. *J. Phys. B At. Mol. Opt. Phys.* **1992**, *25*, 4281. [CrossRef]
23. Bunyan, P.J. The Polarization by Mercury of 1 to 2 keV Electrons. *Proc. Phys. Soc.* **1963**, *81*, 816. [CrossRef]
24. Bunyan, P.J.; Schonfelder, J.L. Polarization by mercury of 100 to 2000 eV electrons. *Proc. Phys. Soc.* **1965**, *85*, 455. [CrossRef]
25. Fink, M.; Yates, A.C. Theoretical electron scattering amplitudes and spin polarizations: Selected targets, electron energies 100 to 1500 eV. *At. Data Nucl. Data Tables* **1969**, *1*, 385–456. [CrossRef]
26. Bartschat, K.; Blum, K.; Burke, P.G.; Hanne, G.F.; Scott, N.S. The fine-structure effect in the low-energy scattering of electrons on Hg and Tl atoms. *J. Phys. B At. Mol. Phys.* **1984**, *17*, 3797. [CrossRef]
27. Haberland, R.; Fritsche, L. On the elastic scattering of low-energy electrons by Hg, Tl, Pb and Bi atoms. *J. Phys. B At. Mol. Phys.* **1987**, *20*, 121. [CrossRef]
28. McEachran, R.P.; Stauffer, A.D. Spin polarisation of electrons elastically scattered from mercury. *J. Phys. B At. Mol. Phys.* **1987**, *20*, 5517. [CrossRef]
29. Sienkiewicz, J.E. Spin polarisation and differential cross sections in elastic low-energy scattering of electrons from mercury. *J. Phys. B At. Mol. Phys.* **1990**, *23*, 1869. [CrossRef]
30. Fritsche, L.; Kroner, C.; Reinert, T. A consistent relativistic theory of electron scattering by atoms. *J. Phys. B At. Mol. Phys.* **1992**, *25*, 4287. [CrossRef]
31. Kelemen, V.I.; Remeta, E.Y. Critical minima and spin polarization in the elastic electron scattering by the mercury atoms. *J. Phys. B At. Mol. Phys.* **2012**, *45*, 185202. [CrossRef]
32. Haque, A.K.F.; Haque, M.M.; Bhattacharjee, P.P.; Uddin, M.A.; Patoary, M.A.R.; Hossain, M.I.; Basak, A.K.; Mahbub, M.S.; Maaza, M.; Saha, B.C. Relativistic calculations for spin-polarization of elastic electron—Mercury scattering. *J. Phys. Commun.* **2017**, *1*, 035014. [CrossRef]

33. Adibzadeh, M.; Theodosiou, C.E. Elastic electron scattering from inert-gas atoms. *At. Data Nucl. Data Tables* **2005**, *91*, 8–76. [CrossRef]
34. Adibzadeh, M.; Theodosiou, C.E. Elastic electron scattering from Ba and Sr. *Phys. Rev. A* **2004**, *70*, 052704. [CrossRef]
35. Adibzadeh, M.; Theodosiou, C.E.; Harmon, N.J. Elastic Electron Scattering from Be, Mg, and Ca. *Atoms* **2024**, *12*, 33. [CrossRef]
36. Mayne, K.I. Polarized electron beams. *Contemp. Phys.* **1969**, *10*, 387–412. [CrossRef]
37. Sherman, N. Coulomb Scattering of Relativistic Electrons by Point Nuclei. *Phys. Rev.* **1956**, *103*, 1601–1607. [CrossRef]
38. Kessler, J. Electron Spin Polarization by Low-Energy Scattering from Unpolarized Targets. *Rev. Mod. Phys.* **1969**, *41*, 3–25. [CrossRef]
39. Kessler, J. *Polarized Electrons*; Springer: Berlin/Heidelberg, Germany, 1976.
40. Salvat, F.; Fernández-Varea, J.; Williamson, W. Accurate numerical solution of the radial Schrödinger and Dirac wave equations. *Comput. Phys. Commun.* **1995**, *90*, 151–168. [CrossRef]
41. Furness, J.B.; McCarthy, I.E. Semiphenomenological optical model for electron scattering on atoms. *J. Phys. B At. Mol. Phys.* **1973**, *6*, 2280. [CrossRef]
42. Bates, D.R. The quantal calculation of the photo-ionization cross-section of atomic potassium. *Proc. R. Soc. Lond. Ser. A. Math. Phys. Sci.* **1947**, *188*, 350–357. [CrossRef]
43. Migdalek, J.; Kim, Y.K. Core polarization and oscillator strength ratio anomaly in potassium, rubidium and caesium. *J. Phys. B At. Mol. Phys.* **1998**, *31*, 1947. [CrossRef]
44. Kolb, D.; Johnson, W.R.; Shorer, P. Electric and magnetic susceptibilities and shielding factors for closed-shell atoms and ions of high nuclear charge. *Phys. Rev. A* **1982**, *26*, 19–31. [CrossRef]
45. Bostock, C.J.; Berrington, M.J.; Fursa, D.V.; Bray, I. Relativistic and Close-Coupling Effects in the Spin Polarization of Low-Energy Electrons Scattered Elastically from Cadmium. *Phys. Rev. Lett.* **2011**, *107*, 093202. [CrossRef] [PubMed]
46. Fano, U.; Theodosiou, C.E.; Dehmer, J.L. Electron-optical properties of atomic fields. *Rev. Mod. Phys.* **1976**, *48*, 49–68. [CrossRef]

Disclaimer/Publisher's Note: The statements, opinions and data contained in all publications are solely those of the individual author(s) and contributor(s) and not of MDPI and/or the editor(s). MDPI and/or the editor(s) disclaim responsibility for any injury to people or property resulting from any ideas, methods, instructions or products referred to in the content.